



University of
Stavanger

Faculty of Science and Technology

MASTER'S THESIS

Study program/ Specialization: Mechanical Engineering	Spring semester, 2014 Open / Restricted access
Writer: Nick Svendsen (Writer's signature)
Faculty supervisor: Hirpa G. Lemu External supervisor(s):	
Thesis title: Dynamic analysis of damping system in FS car using ADAMS Multidynamics Simulations	
Credits (ECTS): 30	
Key words: <ul style="list-style-type: none">- ADAMS/Car- Multidynamic simulation- Design load- Suspension components- Suspension properties	Pages: vii + 45 + enclosure: ix + 6 Stavanger, 12.06.2014 Date/year

Abstract

The aim of this thesis is to use manual calculations, ADAMS/Car and other CAE software to analyze the dynamic of the suspension system for Formula Student car. Manual calculations have been done to find the suitable suspension design load, such as normal, lateral and longitudinal load. The importance of software analysis is to get more accurate results which can be used to build the actual race car. The challenge is to design the 3D model of the car, use the coordinates to build similar model in ADAMS/Car and simulate to find out the optimum suspension properties such as roll center, scrub radius, camber, caster and toe angle.

Results from manual calculations reveal that highest load at front wheel can be up to 3.1 kN, occurs during cornering. At the rear wheel highest load can be up to 3.0 kN during acceleration. Normal load will be transferred through push-rod with safety factor taken into account. Force can be nearly as high as 3.9 kN at the front and 7.3 kN at the rear push-rod. The big difference is due to 35° angle at the front compared to 17° angle at the rear push-rod.

Results from software simulation have shown that camber angle of 2° is enough to maintain good contact patch between the tires and the ground. Caster angle of 5° combined with 0.5° toe-out will enhance the cornering ability of the car. Scrub radius has shown to be 57.5 mm which is slightly higher than expected. When taken into account the minimum wheel travel requirement, the suspension properties changed by only few percent. It is proven that the suspension geometry has been design properly and should be followed while building the actual race car.

Acknowledgement

This thesis was carried out to fulfill the Master degree in Mechanical Engineering at the Department of Structural and Material Science at University of Stavanger, Norway. I would like to express my gratitude to my supervisor Associate Professor Hirpa G. Lemu for his support, supervision and guideline. His knowledge, technical advices and experiences has been very helpful during this period.

I would also like to take this opportunity to express my gratitude to Dr. Jan Kåre Bording, Martin Bae, Tor Gulliksen, Jan Magne Nygård and every team members of Formula Student representing University of Stavanger for the support at the workshop.

Last but not least I would like to express my sincerely to my family, mother and father. Their love and support have been the greatest motivation to overcome the challenges that I've been facing in the last 5 and a half months.

Contents

1. Introduction.....	1
1.1 Background.....	1
1.2 Objective.....	1
1.3 Limitations	2
2. ADAMS/Car software	3
2.1 Introduction.....	3
2.2 Multi-body system.....	3
2.3 Application	4
3. Principle of weight distribution	6
3.1 Wheelbase	6
3.2 Vehicle track	7
3.3 Tire friction coefficient.....	8
3.4 Load distribution	9
3.5 Lateral weight transfer	12
3.6 Longitudinal weight transfer	12
4. Suspension design load	13
4.1 Design case.....	13
4.1.1 Acceleration design case	13
4.1.2 Braking design case.....	14
4.1.3 Cornering design case	14
4.2 Lateral load.....	15
4.3 Longitudinal load.....	19
4.4 Safety factor	20
4.5 Chapter summary	21
5. Suspension components	22
5.1 A-arm.....	22
5.2 Push-rod.....	24
5.2.1 Push-rod and pull-rod.....	24
5.2.2 Load through push-rod.....	24
5.2.3 Push-rod design capacity	25
5.3 Rocker	26
5.4 Spring and damper.....	27

5.5 Anti-roll bar.....	28
5.6 Chapter summary	29
6. Suspension properties and simulations.....	30
6.1 Introduction.....	30
6.2 Roll center.....	30
6.2.1 Determining roll center	30
6.2.2 Roll center movement.....	30
6.2 Camber.....	32
6.3 Caster angle.....	35
6.4 Toe	37
6.4.1 Bump steer.....	37
6.4.2 Roll steer.....	38
6.5 Scrub radius	39
6.6 Chapter summary	41
7. Conclusion and future work.....	43
7.1 Conclusion	43
7.2 Future work.....	43
References.....	44
Appendix A: Material properties	i
A.1 Steel.....	i
A.2 Aluminum.....	i
Appendix B: Input for ADAMS/Car	ii
B.1 Front suspension coordinates	ii
B.2 Rear suspension coordinates.....	iii
B.3 Parallel wheel travel.....	iv
B.4 Opposite wheel travel.....	iv
B.5 Constant corner.....	v
Appendix C: Eurocode 3.....	vi

List of Figures

Figure 1: Comparison between FORTRAN and C++.....	3
Figure 2: Multi-body system	4
Figure 3: Different stages of ADAMS application	5
Figure 4: Steering angle for a car different wheelbase	6
Figure 5: Wheelbase and vehicle track of 2014 car	7
Figure 6: Front tire friction coefficient at 7° slip angle.....	8
Figure 7: Rear tire friction coefficient at 7° slip angle	8
Figure 8: Longitudinal, lateral and normal force acting to the tire	9
Figure 9: Components location	10
Figure 10: Weight distribution of 2014 car.....	11
Figure 11: Skid-pad event layout	15
Figure 12: Model of left handed constant corner simulation	18
Figure 13: Constant corner analysis	18
Figure 14: Front and rear right a-arm (yellow).....	22
Figure 15: Upper and lower A-arm angle (β) horizontal to the ground.....	23
Figure 16: A-arm angle (α) with bearing housing and bearing.....	23
Figure 17: Push-rod vs pull-rod configuration	24
Figure 18: Front and rear rocker.....	27
Figure 19: Öhlins TTX 25 damper with spring.....	28
Figure 20: Anti-roll bar designed by M. Åsland.....	29
Figure 21: Front view suspension roll center	30
Figure 22: Front suspension lateral roll center	31
Figure 23: Front suspension vertical roll center.....	31
Figure 24: Camber angle at front wheel.....	33
Figure 25: Camber during constant corner simulation	33
Figure 26: Front camber during opposite wheel travel	34
Figure 27: Left view of the car with positive front caster.....	35
Figure 28: Front caster of opposite wheel travel.....	36
Figure 29: Front caster during parallel wheel travel	36
Figure 30: Illustration of toe-in and toe-out.....	37
Figure 31: Bump steer caused by parallel wheel travel	38
Figure 32: Roll steer caused by opposite wheel travel	39
Figure 33: Front view scrub radius	40
Figure 34: Change in scrub radius when steering angle change.....	40
Figure 35: Change in kingpin inclination angle with different steering angle.....	41

List of Table

Table 1: Front sprung and unsprung mass comparison.....	10
Table 2: Rear sprung and unsprung mass comparison	11
Table 3: The 2014 car load parameters	13
Table 4: Input for calculation of lateral load.....	16
Table 5: Mass transfer and lateral load.....	17
Table 6: Longitudinal load input	19
Table 7: Longitudinal load results	20
Table 8: Load including 1.5 in safety factor taken into account.....	20
Table 9: A-arm dimensions and geometries	22
Table 10: Push-rod and pull-rod comparison	24
Table 11: Force through push-rod.....	25
Table 12: Push-rod tube dimension	26
Table 13 : Input values for calculation of buckling capacity.....	26
Table 14: Output for buckling capacity.....	26
Table 15: Motion ratio of front and rear rocker	27

Abbreviations

ARB	Anti-roll bar
CoG	Center of Gravity
CAD	Computer-aided design
CAE	Computer-aided engineering
FS	Formula Student
FSAE	Formula Society of Automotive Engineers
MBD	Multibody Dynamics
RC	Roll Center
SF	Safety Factor

1. Introduction

1.1 Background

Formula Student competition started in 1998 with 4 teams participating. In 2014, 16 years later, there are over 130 teams, in which 3 of them representing Norway. The competition is open for university from all around the world to participate. In Europe, several well-known locations such as Silverstone Circuit (UK), Hockenheimring (Germany) and Red Bull Ring (Austria) will be hosting Formula Student competition. The competition also taken place in USA, Asia and Australia but due to limited founding and time available the team has chosen to participate at Silverstone Circuit.

For University of Stavanger the Formula Student project started in 2012 by a group consists mostly of bachelor students, most of them are genuinely interested in motorsports. The number of students interested to take part in the project increases each year. This year, there are 14 students who write their thesis about the car. The biggest challenges about this year car compared to previous years are carbon fiber monocoque chassis design and electrical engine. This is the first time the team will be building a race car with in-wheel electrical engine. For this reason, the team has expanded to recruit students from several institutes to strengthen the teamwork and knowledge across different engineering discipline.

The background for the project as a whole is to combined theoretical knowledge with practical skills and realizes the concept. It is often that students with engineering degrees graduate from university with very limited practical knowledge. Being part of the project means that each team member knows how to implement “theory into practice” by learning the manufacturing process of each component and also build the car. Each team member will also learn how to work and function as a team in a deadline oriented environment.

The background for the thesis is to understand the suspension system of a race car. There are several types of suspension system and how it can be setup to give optimal working range. Testing of previous year car reveals that the car tends to lift its inner wheel while cornering. With this in mind, the thesis will be focus on improving the suspension system and the car behavior on the race track which can be done more accurately by using ADAMS software.

1.2 Objective

The main objective of the Formula Student project is to design, analyze and manufacture a proper race car. The goal is to pass a series of scrutineering, tests, as well as static and dynamic events including:

- Business presentation
- Engineering design presentation
- Cost report analysis
- Acceleration event
- Skid-Pad event
- Autocross (sprint)
- Endurance and efficiency

The ultimate goal for the team is to finish every single race and placed among top 30.

The main objective of the thesis is to understand and explain the theory, properties and importance of the good suspension system of a race car, which will be shown in Chapter 3 to Chapter 6. Once the suspension theory and properties are in place, the next goal is to show the design and simulation of the components and geometry in multidynamic software for compatibilities. The aim is to build lighter components than previous years while improving the properties of the car during cornering, accelerating and braking. Optimal suspension setup will reduce the car roll, gives better load transfer to the damper and helps maintain contact patch between the tires and the ground.

This thesis will cover the following suspension components:

- A-arm
- Push-rod
- Rocker
- Spring and damper

The thesis will also cover the suspension properties, such as:

- Roll center
- Camber angle
- Caster angle
- Toe
- Scrub radius

1.3 Limitations

Suspension system is a huge and complex part of the car. The team has several students working on different components of the suspension assembly. For this reason, several suspension components and parts will not be including in this thesis, such as:

- Anti-roll bar
- Upright
- Hub
- Rim and tires

2. ADAMS/Car software

2.1 Introduction

ADAMS is the most well-known Integrated Solution product of MSC Software. It is the world's most widely used Multibody Dynamics software (MBD) with graphical interface which allows engineers to be able to modeling and simulating in 3D. By using ADAMS/Car the suspension kinematics and dynamics can be evaluate before building physical prototype. This will help to reveal problems during the early stage and will most likely save costs for the team.

The foundation of ADAMS/Car is:

- Adams/View
- Adams/Solver
- Adams/Postprocessor.

These are the base modules to view the graphics and animations, solve the dynamic simulations, plot into graphs and convert the CAE data to be used to produce the machined parts. ADAMS uses the FORTRAN and C++ numerical solvers. Implementation of C++ technology enhances the performance of the solver and allows more features [1].

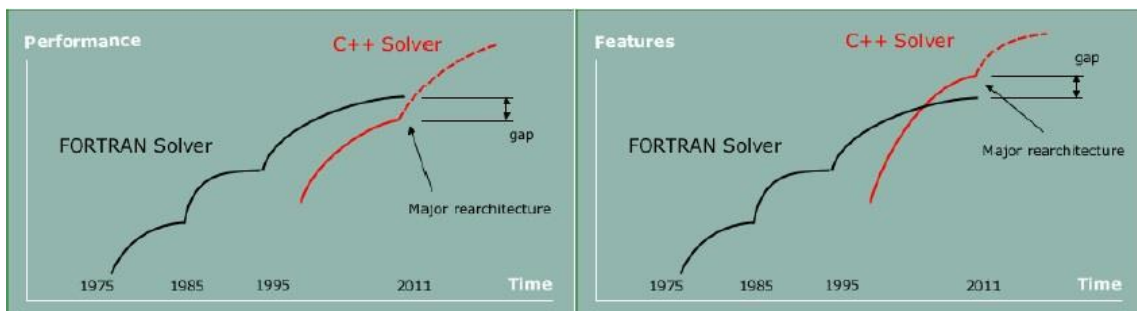


Figure 1: Comparison between FORTRAN and C++

Image courtesy of J.L. Ortiz

Figure 1 shows how different solver evolving through time. While FORTRAN has been available for much longer than C++ Solver, the technology is on its third stagnation point. C++ Solver is on its re-architecture stage and is expected to close the performance gap and extend the features gap compared to FORTRAN Solver once the re-architecture stage is finished.

2.2 Multi-body system

The concept of multi-body system is to transform the motion between rotational and translational. The system consists of 2 or more interconnected bodies, formed by a set of rigid solids and linked by kinematical relationships or joints [2]. The system has both kinematics and dynamics term. The kinematics term is the motion of the bodies, i.e. positions, velocities or accelerations. The dynamics term is the cause or change in motion.

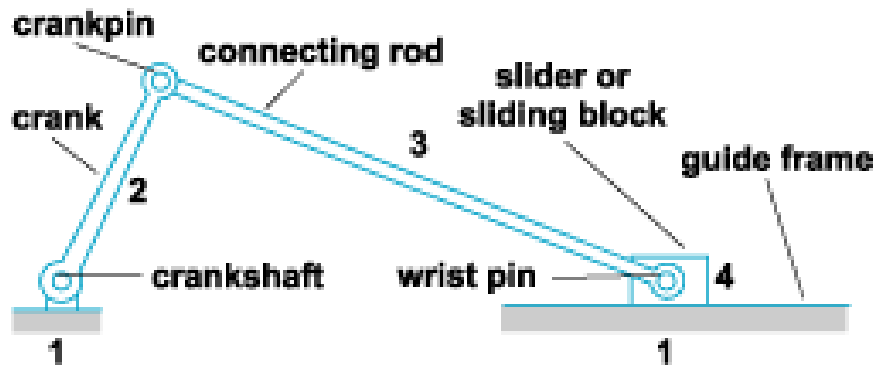


Figure 2: Multi-body system

Image courtesy of The McGraw-Hill Companies, Inc. (2005)

Figure 2 above shows a simplified multi-body system. The system consists of sliding mass (1&4) and rigid crank (2) which is connected by a connection rod (3). The CAE software MSC Adams is designed especially for multi-body system.

2.3 Application

Adams is optimized for large scale problems. The result is improving engineering efficiency and reduces costs. The software is applicable for wide range of industries such as aerospace, energy, oil & gas and automotive. In this thesis, the application of ADAMS/Car will be mainly use for FS 2014 suspension design.

The software makes it possible to create the 3D geometry file from scratch using ADAMS. However, MSC software has provided a FSAE template, called FSAE 2012, with pre-modeled vehicle geometry. The hard-point, mass, tires and spring properties have to be redefined to match the CAD file from Autodesk Inventor. Once the hard-point matches, the result of the simulation should give the numerical values close to expected values.

The application of the Adams/Car will be used to fine-tune the suspension geometry. The suspension links which is a multi-body system will be check for compliance between each other. The suspension setup and some steering properties will be analyzed to find flaw of the designed suspension system. The load analysis will also be analyzed to find the proper linear and nonlinear results.

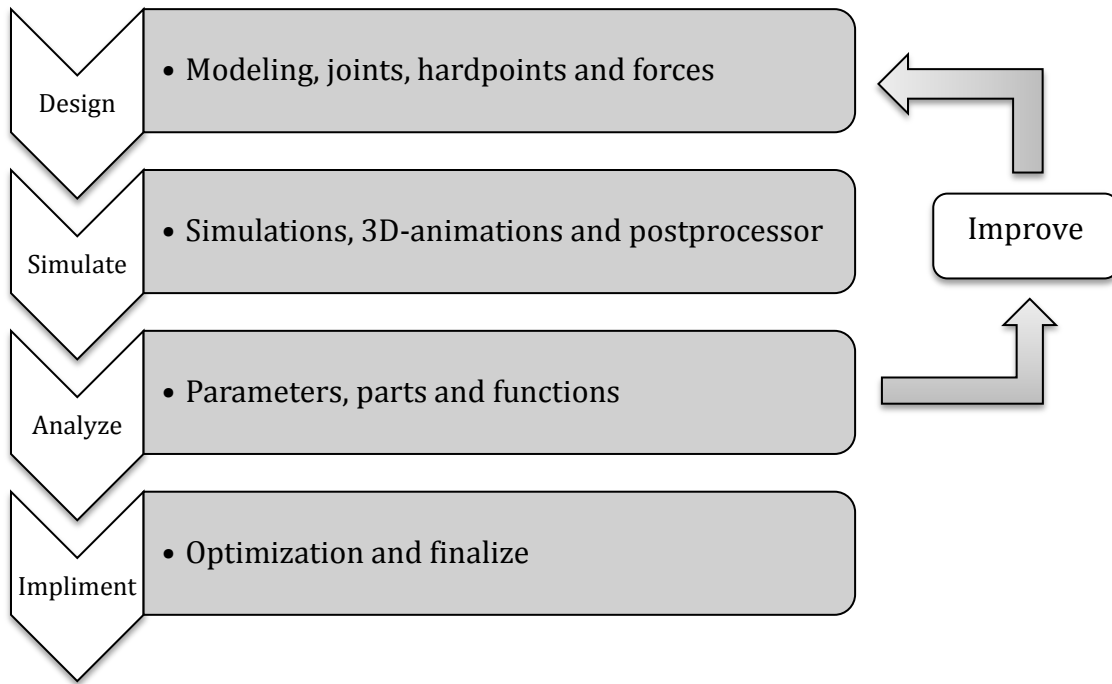


Figure 3: Different stages of ADAMS application

Figure 3 shows that the application of ADAMS can be summarized in 4 different stages. During the design phase the designer can choose to create the modeling geometry from scratch or use exiting model that has been created. Once the model is completed, the designer can apply the necessary forces and constraints. During simulation phase the computer uses numerical solvers to calculate the given parameters. The designer can also use animation feature to see how the model behave dynamically. The results of simulation can be presenting in graphical format. In analyzing stage, the data and parameters have to be check carefully for compatibility. If unexpected results or errors are shown, then the whole system has to be reevaluated. After achieving the satisfying results the model can be finalize and put into reality by building a prototype or scale test model.

3. Principle of weight distribution

3.1 Wheelbase

Wheelbase of the vehicle is defined as the distance between the center of the front wheel and the rear wheel, usually expressed in mm or inches. FSAE rules for 2014 states that the vehicle must have a wheelbase of at least 1525 mm (60 inches) [3]. For race car in general, wheelbase length affected the car differently in fast and slow corners. The general assumption is that shorter cars tends to be faster around slow, shorter corners while longer cars are faster around fast, longer corners. In reality the difference between longest and shortest cars varies by only a tiny fraction of a second [4].

Different wheelbase also serves the purpose of:

- Weight transfer between front and rear
- Ability to move around an axis
- Steering angle needed in a corner.

During acceleration and braking the weight of the car will be transfer longitudinally between front and rear axle. Longer wheelbase reduce the effect of weight transfer, hence less force variation is needed to react by the suspension systems. This allowed the suspension to be softer. Less weight transfer between front and rear axle allowed the driver to brake later and harder before going into the corner and also improve straight line stability. Long wheelbase has negative effect of increase weight due to longer span between front and rear axle [5]. Another negative effect of long wheelbase is the effort the driver has to put into steering during cornering. Longer vehicle needed more steering angle to be able to rotate around an axis, as illustrate in Figure 4 below.

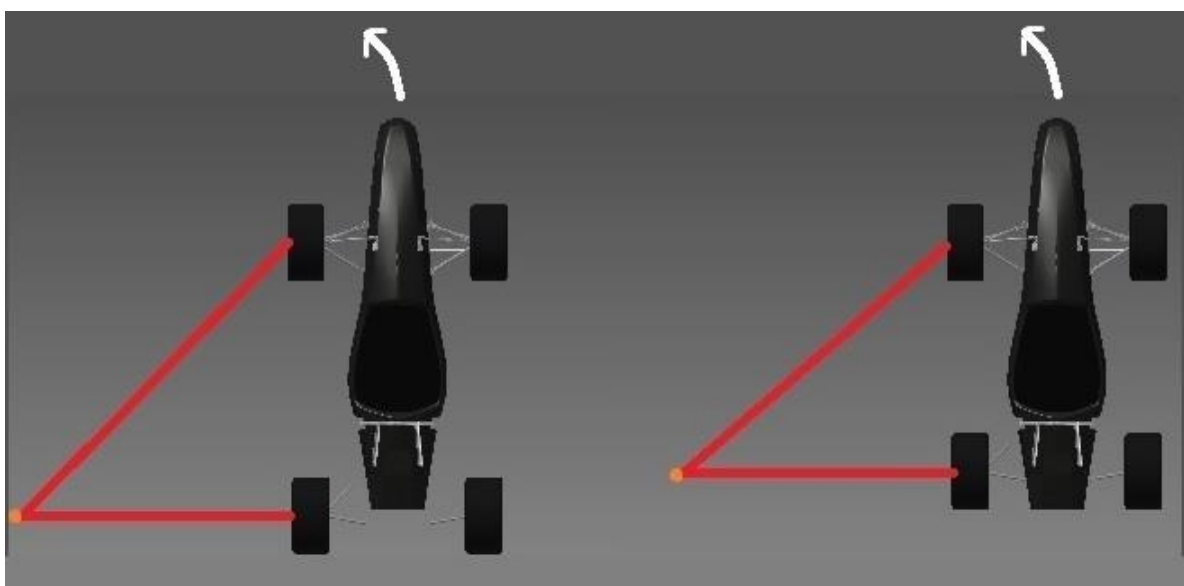


Figure 4: Steering angle for a car different wheelbase

Wheelbase for 2013 car was set to 1600 mm [6]. However, this year will be set to 1700 mm due to monocoque design combined with the desire of having the rear wheel as far back as possible while maintaining a reasonable gap between the rear tire and sidepods. Illustration of wheelbase is shown in Figure 5 below.

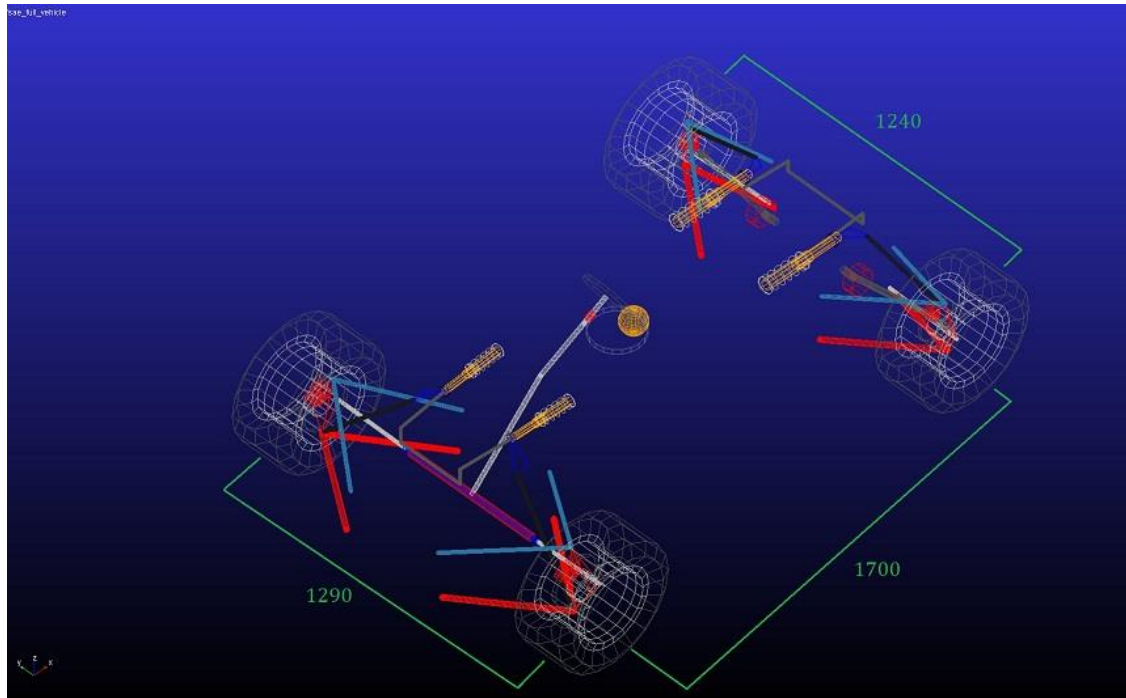


Figure 5: Wheelbase and vehicle track of 2014 car

3.2 Vehicle track

Vehicle tracks defined as the distance between the left and right tire, measured from the centerline and usually expressed in either mm or inches. FSAE rule for 2014 states that the smaller track must not be less than 75% of the larger track. The effect of the vehicle track is similar to the length of the wheelbase. However, the weight transfer will be in lateral direction between left and right tire instead of longitudinal direction. Wider track allows less weight transfer between left and right side which allows cornering at higher g-force.

The negative effect of wide vehicle track is increase weight of suspension components as well as reduces cornering ability for narrow race track. In this case, the designer must exploit as much width as possible. This method has been done several times before by making the front track wider than the rear. During braking into cornering, the load is transferred diagonally from inside the rear tire to outside of the front tire which improve the cornering ability of the vehicle.

Vehicle track for 2013 car was set to 1290 mm at the front and 1240 mm at the rear, as illustrated in Figure 5. This gives a mean track of 1265 mm. The monocoque body of this year car is slightly narrower than last year steel space frame body. However, the vehicle track will remain the same to maintain balance between stability in high g-force corner and cornering ability in narrow part of the race track.

3.3 Tire friction coefficient

Weight transfer between front and rear and side to side will cause different load to the tires. Load sensitivity is proportional with friction coefficient of the tire. The heavier the tire is loaded, the less coefficient of friction will be for that particular tire and vice versa [7].

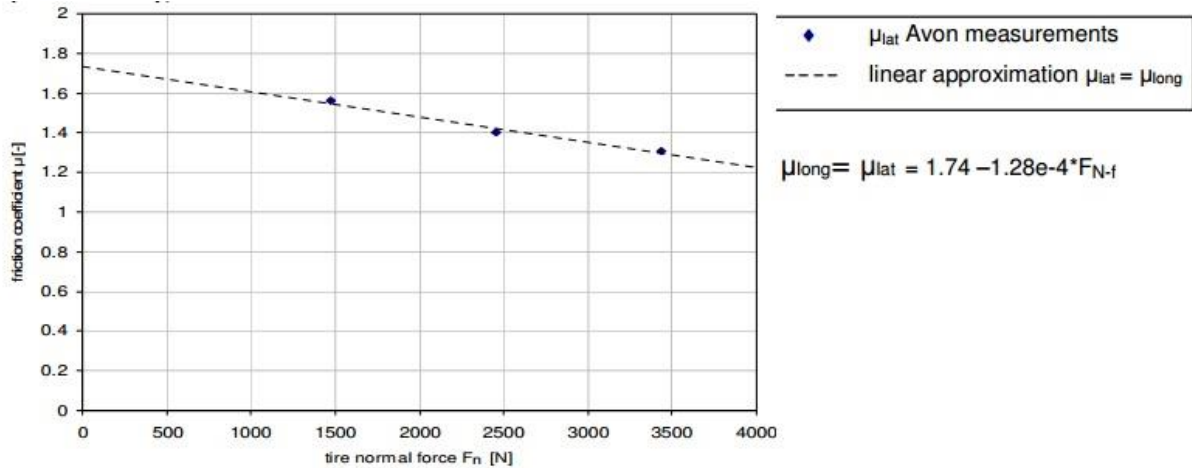


Figure 6: Front tire friction coefficient at 7° slip angle

Image courtesy of van Berkum (2006)

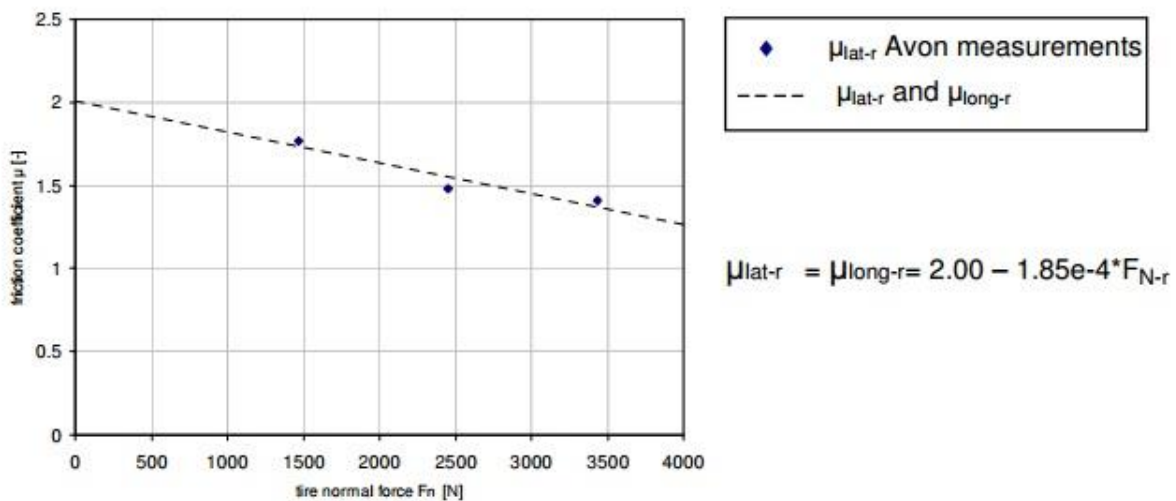


Figure 7: Rear tire friction coefficient at 7° slip angle

Image courtesy of van Berkum (2006)

Figure 6 and 7 shown that for 7° slip angle the rear tires have higher friction coefficient than front tires. Hoosier tires and Avon tires are quite similar hence the tires coefficient values from Berkum can be used.

In 2012 the team bought enough set of Hoosier tires for several years ahead. However, rubber is perishable hence the quality of 2014 tires may not be the same as 2 years ago. It is also worth mention that for formula 1 tire, the friction coefficient of slick tires is usually between 1.0 and 1.7 [8][9]. With these 2 factors taken into consideration, the

friction coefficient is expected to be lower than the values taken from van Berkum. However, due to lack of proper testing and equipment for measurements, the values from van Berkum's work will be used for future calculations.

3.4 Load distribution

Load distribution of the vehicle is the load that transfers to the tire contact patch to the ground. The normal force reacts upward from the ground to keep the vehicle in equilibrium. Load distribution gets more complicated if the vehicle is under acceleration, braking or cornering.

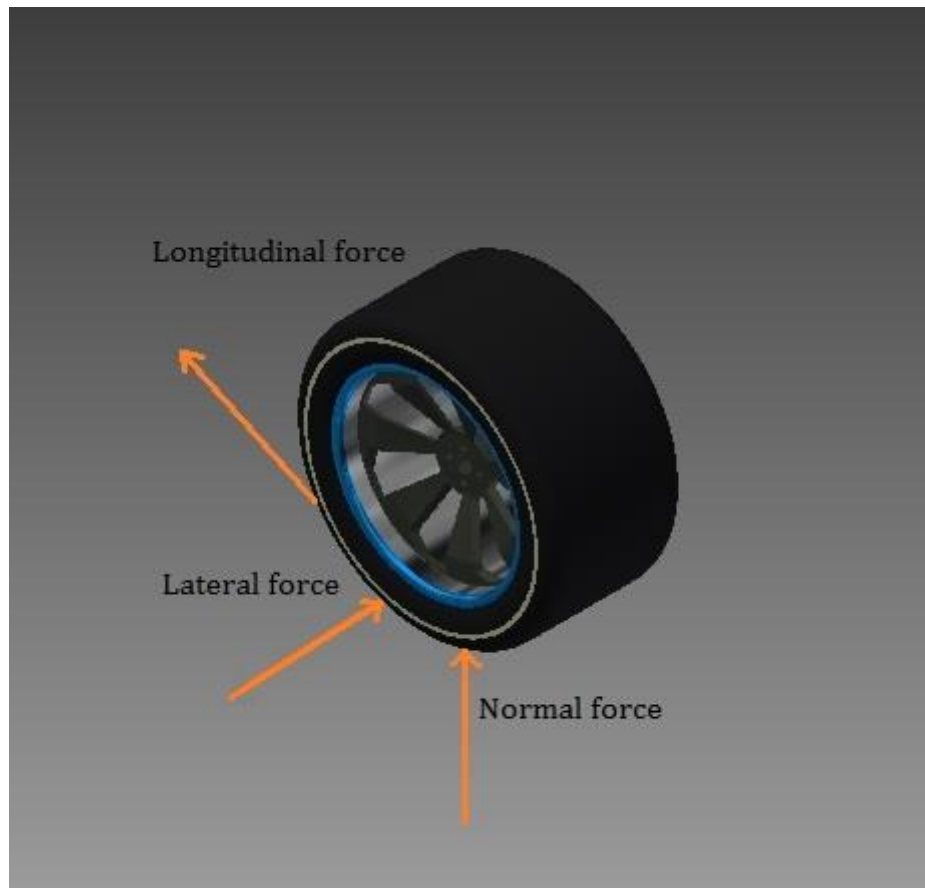


Figure 8: Longitudinal, lateral and normal force acting to the tire

Figure 8 shows how different forces acting between the ground and the tire. Longitudinal force is the force acting toward the front and rear of the car. Lateral force is the force acting to the side of the car and normal force is the force from the surface acting upward to the tire.

Suspension geometry and CoG play a huge role in vertical load distribution. It is critical that the CoG of the vehicle has to be located as close to the ground as possible. Increasing the height of CoG will result in increased in load transfer. Under braking the height of CoG and front a-arm geometry determines the dive characteristic at the front of the car while rear a-arm geometry determines the squat characteristic during acceleration.

For 2014 car, the team has aimed for vertical load distribution somewhere between 40/60 and 45/55 between front and rear, depending on the battery placement. Due to the car is rear wheel drive, it is desire to have the static weight toward the rear end. The unsprung mass at the front and rear end of the car is shown in Table 1 and 2 respectively.

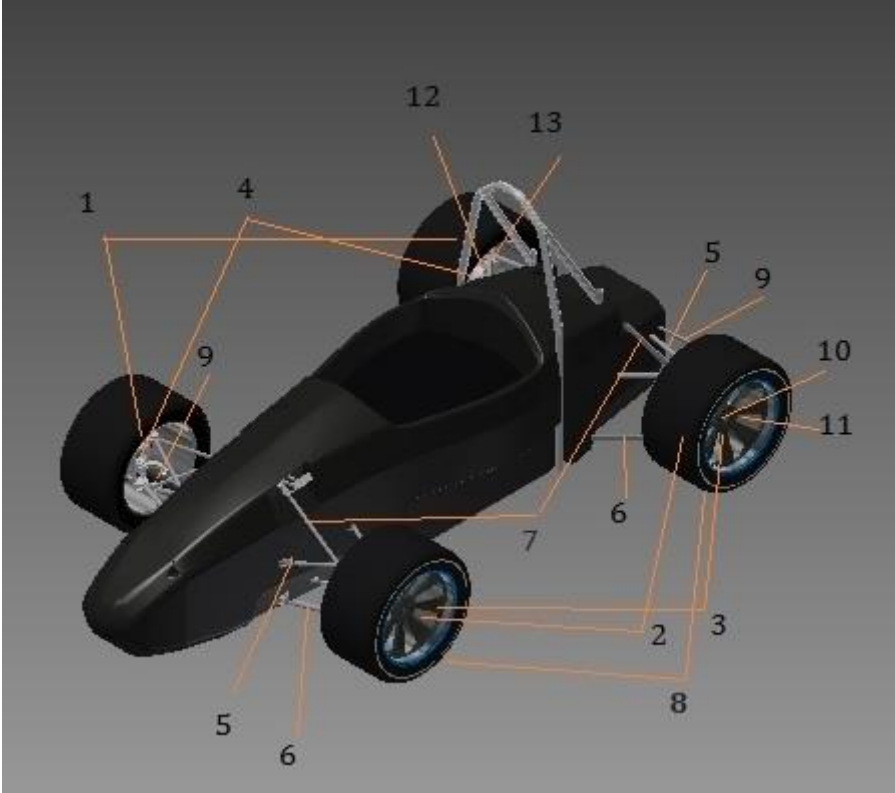


Figure 9: Components location

Table 1: Front sprung and unsprung mass comparison

Front components	2013 (kg)	2014 (kg)	% change
1. Uprights + brackets	2.24	2.22	-0.89
2. Brake disc	0.98	0.97	-1.38
3. Brake system	1.42	1.42	0.00
4. Hub ¹	0.53	1.83	244.11
5. Upper a-arm ²	0.96	0.55	-42.40
6. Lower a-arm ²	1.21	1.13	-6.91
7. Pushrod ²	0.70	0.35	-49.76
8. Wheel	16.52	16.52	0.00
9. Tie rod ²	0.70	0.32	-54.57
Unsprung	23.49	24.14	2.78
Sprung	1.79	1.18	-34.22

¹ Calculated with Aluminum hub for 2013 and steel hub for 2014

² Assumed that half of the total mass to be unsprung

Table 2: Rear sprung and unsprung mass comparison

Rear components	2013 (kg)	2014 (kg)	% change
1. Uprights + brackets	2.24	5.80	158.70
2. Brake disc	0.98	0.97	-1.38
3. Brake system	1.02	1.02	0.00
4. Hub ¹	0.53	1.83	244.11
5. Upper a-arm ²	0.96	1.05	9.17
6. Lower a-arm ²	1.21	1.06	-12.15
7. Pushrod ²	0.70	0.46	-35.32
8. Wheel	16.52	16.52	0.00
9. Toe rod ²	0.25	0.26	6.39
10. Bearing + housing	1.33	1.33	0.00
11. Drive axle ²	0.85	0.00	-100.00
12. Gear	0.00	1.80	-
13. Electric engine	0.00	19.00	-
Unsprung	24.62	49.69	101.85
Sprung	1.99	1.42	-28.66

Table 1 shown that the total unsprung mass has been increased by 0.65 kg. The main reason is the steel hub that was chosen for 2014 car. Table 2 shown that total unsprung mass is approximately 2 times of the amount of 2013 car. The main reason is the electric engine at rear wheels. The planetary gear systems couple with bigger and stronger rear uprights also significantly increases the unsprung mass at the rear. However from the suspension components point of view, the weight saving has been achieved. Total unsprung mass for front and rear is 74.26 kg.

The total mass of the 2014 car is estimated to be 350 kg including 90 kg driver. Weight distribution is shown in figure 3.

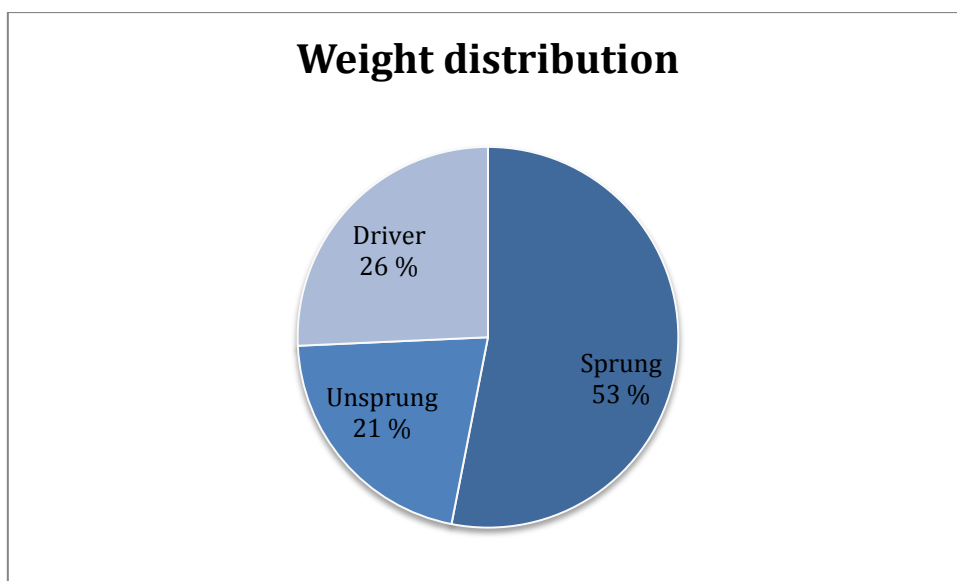


Figure 10: Weight distribution of 2014 car

3.5 Lateral weight transfer

Every vehicle tends to roll during cornering. The car roll is dependent on its CoG, front and rear RC, lateral g-force in cornering and suspension setup [10]. Lateral weight transfer of a vehicle is the weight transfer between the left and right side of the centerline. During cornering the effect of weight transfer will cause the inner tires to lift while outer tires will be press down to the road.

In corner, the centrifugal force will pull outward on an object away from the axis center and draws the vehicle away from the center of rotation [11]. The effect is increasing proportional to CoG height of the car. To keep the car path continually around the center axis of the corner, the friction force from all 4 tires has to react to the centrifugal force. Friction force that act inward to the cornering center is called lateral force, as shown earlier in Figure 8.

3.6 Longitudinal weight transfer

During acceleration and braking the weight of the car tends to shift forward and rearward respectively. Longitudinal weight transfer of a vehicle is weight transfer between the front and the rear of the car, where CoG is the center point. The effect is similar to lateral weight transfer and increased proportional to CoG height of the car.

For a rear wheel drive car, it is desire to have large longitudinal weight transfer when accelerate from stand still. The weight increase at the rear end of the car helps to increase grip and prevent the rear wheels to spin during acceleration. The friction between the tires and the surface creates a friction force in longitudinal direction as shown in Figure 8 above. However, when the car is in motion, longitudinal weight transfer should be as low as possible. The main reason is during heavy braking into a corner. Too much weight transfer to the front end will cause the inner rear wheel to lift into the corner and the result is the car will have less mechanical grip overall.

4. Suspension design load

4.1 Design case

The necessary design load of 2014 car will be based on official results of Formula Student UK 2013 time and scores. The official time of the top teams in different categories will be a benchmark of this year car, due to 2 main reasons:

- Due to the law of diminishing returns, it is more difficult for the team to achieve better results than the first place team.
- The relatively low budget compared to top teams, the car will not have the best technologies (i.e. lightweight engines, optimized battery package, carbon fiber parts etc.) to match those results.

The car will be design for a maximum cornering force, braking force and acceleration force. Some parameters of the 2014 car are shown in Table 3 below:

Table 3: The 2014 car load parameters

Parameters	Values
W [kg]	350
l [mm]	1700
CoG [mm]	300
g-acceleration	1.1
g-brake	1.7
g-corner	1.6

There will not be any aerodynamic package for this year car. The effect of downforce will assumed to be much less significant and will be neglected.

4.1.1 Acceleration design case

The g-force during acceleration was taken from the acceleration event results. The track is 75 m long and the fastest car managed 3.686 seconds [12]. Assumed that the top speed of the fastest accelerating car is 125 km/h. Equation 1 and 2 show how to calculate g-force from acceleration.

$$v = v_0 + aT \quad (1)$$

$$g_{acceleration} = \frac{v^2}{sG} \quad (2)$$

Where:	$g_{\text{acceleration}}$	Acceleration g-force
	v	Top speed
	v_0	Starting speed (0 km/h)
	a	Acceleration
	T	Time the car takes to reach top speed
	s	Track length
	G	Gravitational force.

4.1.2 Braking design case

The g-force during braking was taken from brake test at previous year event. Equation 1 and 3 show how to calculate g-force from braking:

$$g_{\text{brake}} = \frac{-v_{36}^2}{sG} \quad (3)$$

Where:	g_{brake}	braking g-force
	v_{36}	the initial speed before braking (36 km/h)
	s	stopping distance (6 meters)

The negative sign shows the deceleration. To keep it simple, the final value will be defined as positive but the deceleration and force will act the opposite of the acceleration.

4.1.3 Cornering design case

The cornering g-force was taken from the skid-pad event results where the fastest car managed to lap an 8-shaped track in 4.789 seconds [13].

FSAE SKIDPAD LAYOUT

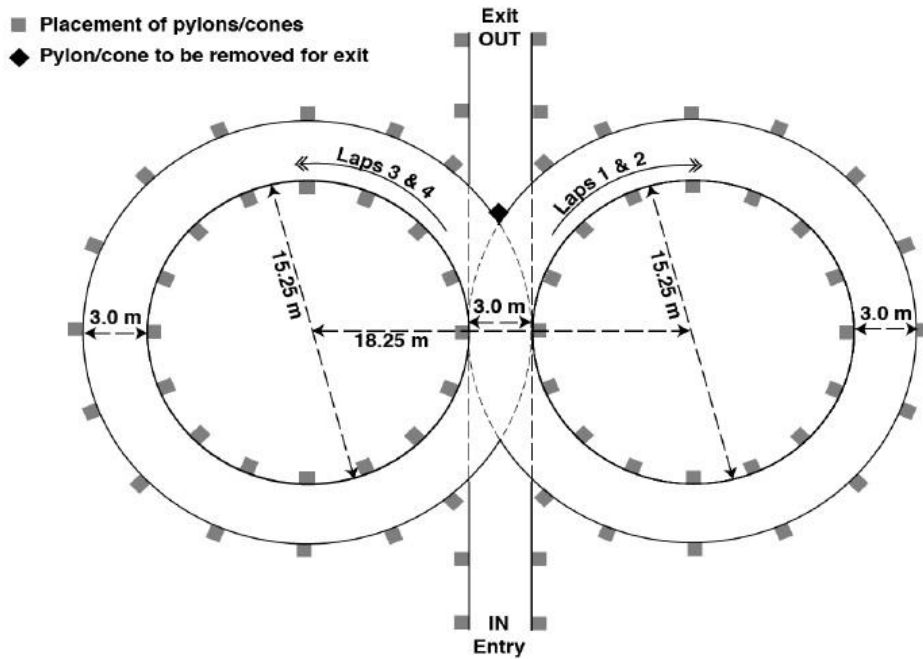


Figure 11: Skid-pad event layout

Image courtesy of SAE International (2014)

Assumed the mean radius of the track is 16.25 meters, the g-force during cornering is calculated by Equation 4 [3].

$$g_{corner} = \frac{2.012 \times D}{T^2} \quad (4)$$

Where:

g_{corner}	Cornering g-force
D	Track diameter, in this case the diameter is set to 18 meters
T	Average time of the right-handed turn and left-handed turn of the event.

4.2 Lateral load

Lateral load is the increasing/decreasing load to the tires when the car is subjected to lateral acceleration. The lateral acceleration causes the lateral weight transfer as described in Chapter 3.5. In corner, the inner front and rear tires will be subjected to reduced load and the tires will have less grip, while the opposite occurs for outer tires. Table 4 shows the input for lateral load.

Table 4: Input for calculation of lateral load

Parameters	Values
A_Y	1.6
h [mm]	300
t_f [mm]	1290
t_r [mm]	1240
W [kg]	350
μ_{eff_f}	1.55
μ_{eff_r}	1.6

Equations 5 to 8 show how to calculate the correct lateral load to each tire [14]:

$$LLT = \frac{A_Y \times h}{t_{front}} \quad (5)$$

Where: LLT Total lateral load transfer as a fraction of total weight
 A_Y g-force while cornering
 h CoG height
 t_{front} Front wheelbase

When calculating mass of the inner wheel

$$M_{i,o} = LLT \pm 0,5 \quad (6)$$

The mass of outer wheel is increased while mass of the inner wheel is reduced while cornering, hence the negative sign for the inner wheel.

Where: $M_{i,o}$ Mass of the inside/outside wheel during cornering

$$Lat_{front} = M \times 9.81 \times \mu_{eff_f} \quad (7)$$

$$Lat_{rear} = M \times 9.81 \times \mu_{eff_r} \quad (8)$$

Where:	Lat_{front}	Lateral load of the front wheel
	Lat_{rear}	Lateral load of the rear wheel
	M	Mass of the specific wheel during cornering
	μ_{eff}	Tire friction coefficient

Given that the steady state, the weight distribution is 50% between left and right tires, the result of lateral load is shown in Table 5 below:

Table 5: Mass transfer and lateral load

		Inner	Outer
Front	% mass	0.13	0.87
	Mass [kg]	20.15	137.35
	Weight [N]	197.63	1347.45
	Lateral load [N]	306.32	2088.55
Rear	% mass	0.11	0.89
	Mass [kg]	21.73	170.77
	Weight [N]	213.21	1675.22
	Lateral load [N]	319.81	2512.82

The effect of the lateral load at outer front wheel will always be more than the lateral load at outer rear wheel. The reason is the effect of the centrifugal force combined with distance between CoG and roll center at front/rear end of the car. In this case, the rear lateral load in reality will be less than the values from Table 5 and the values can be neglected.

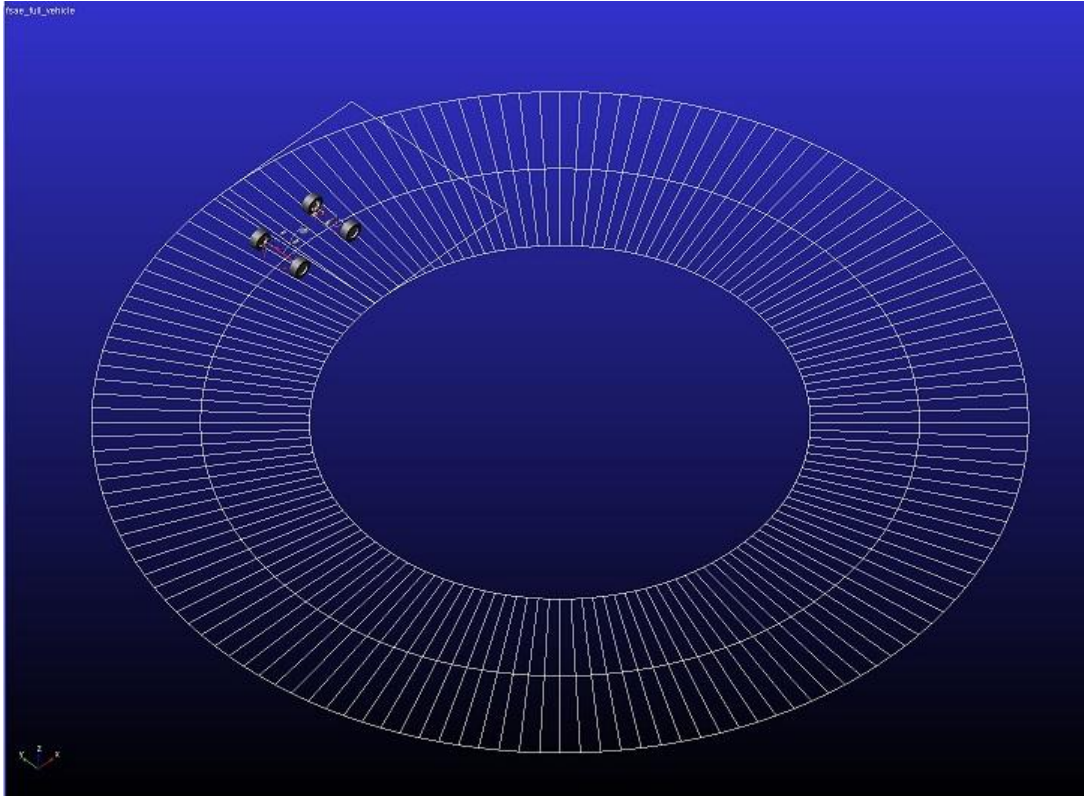


Figure 12: Model of left handed constant corner simulation

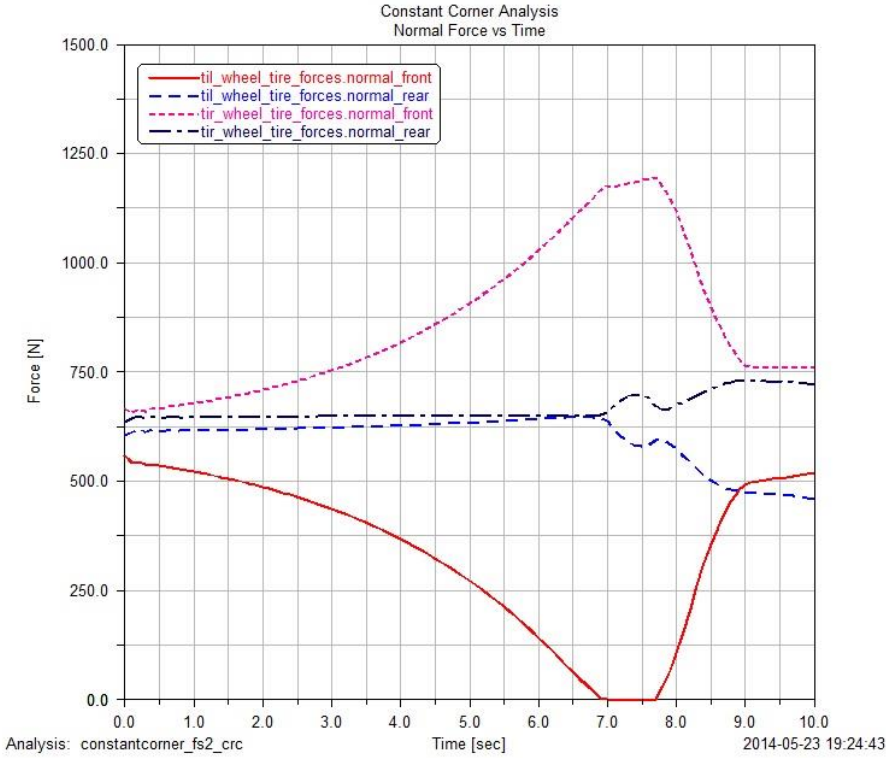


Figure 13: Constant corner analysis

Figure 13 shows that ADAMS/Car simulation confirms that normal forces at rear tires will not exceed normal forces at front tires. In this simulation, the car is doing a left hand turn at 0.5g at the initial time and end at 1.6g. In this case the normal forces at outer tires (right) are gradually increasing while at inner tires (left) the normal forces are gradually decreasing. Force peaked at around 1200 N when the car stop turning due to tires slip. The simulation shows the importance of good tires friction coefficient and suspension setup to transfer the transverse load. In this simulation, the tire data have not been changed from default due to lack of testing and lack of proper tires data input.

4.3 Longitudinal load

Longitudinal load is load to the tires when the car is subjected to longitudinal acceleration. During acceleration the load will be less at the front and opposite during braking. The tires with reduced load will have less grip overall. The longitudinal load during acceleration for this car is limited to the grip between rear tires and the road, while under braking the car brakes with all 4 wheels with 70/30 front and rear ratio.

Table 6 shows the input for longitudinal load:

Table 6: Longitudinal load input

	Acceleration	Brake
a/g	1.1	1.7
h	300	300
l	1700	1700
W	350	350
W ₁	157.5	157.5
W ₂	192.5	192.5
u _{eff_f}	1.68	1.55
u _{eff_r}	1.55	1.68

Equations 9 and 10 show how to calculate longitudinal load to each tire during braking and accelerating [14].

$$W_{f,r} = (W_1 \pm W \frac{a h}{g l}) \times 9.81 \quad (9)$$

Where:	W _{f,r}	Weight of front/rear wheel
	W ₁	Mass distribution at front wheel
	W	Total mass of the car
	a/g	g-force
	l	Vehicle track

The plus sign indicates that weight transferred to the particular wheel, opposite for the minus sign.

$$F_{long} = \frac{W_{f,r} \times \mu_{eff}}{2} \quad (10)$$

Where: F_{long} Longitudinal force

The actual longitudinal load is when the friction coefficient is taken into account. Table 7 shows the result of longitudinal load of each front and rear wheel during acceleration and braking.

Table 7: Longitudinal load results

		Acceleration	Brake
Front	Weight [N]	439.286	1287.563
	Longitudinal load [N]	738.0005	1995.722
Rear	Weight [N]	1277.464	429.1875
	Longitudinal load [N]	1980.069	721.035

The car is slightly heavier at the rear but due to higher g-force during braking there will be slightly more reaction force at the front wheels.

4.4 Safety factor

As mentioned in Chapter 4.1 Design case, the car will very unlikely to managed the designed g-force. Due to engineering discipline, the car has to be design to be able to withstand slightly higher load than expected to allow for emergency situations. The unexpected load may occurs from hitting a bump while cornering, under heavy braking or when the car hitting the cone.

Safety factor is a safety gap between the real and calculated values of material strength and the amount of operating stresses [15]. With the proper amount of safety factor, the design may be considered high quality and reliable with regards to design load, material properties and performance [16]. For this thesis, the safety factor of 1.5 will be used. This value is chosen because it gives sufficient amount of safety without adding too much unnecessary weight to the car. Table 8 shows the important lateral and longitudinal load including safety factor.

Table 8: Load including 1.5 in safety factor taken into account

Location	Load type	Load with 1.5 SF
Front (outer wheel)	Lateral [N]	3132.82
Rear	Longitudinal [N]	2970.10

4.5 Chapter summary

Design load was based on the official results from the top teams. It is highly unlikely that the 2014 car from University of Stavanger will surpass the time achieved by the top team due to lower budget and less technological equipment to build stronger and lighter parts.

The design load criteria will be based on braking test as well as acceleration and skid-pad events. When the car is accelerating, the longitudinal load will cause the weight transfer to the rear wheel. Each rear wheel will subject to longitudinal load of up to 2970.1 N with 1.5 safety factor.

Load at front wheel can either occurs when cornering or braking. Calculations have shown that lateral load occurs while cornering is higher than longitudinal load that occurs while the car is under heavy braking. In this case, the front suspension of the car will be design to withstand lateral load of 3132.8 N with 1.5 safety factor.

5. Suspension components

5.1 A-arm

A-arm or double wishbone-arm is one of the most important suspension components of a race car. A-arm helps transferring the load from the tires into the chassis, depending on the geometry. For open-wheel race car, the a-arm suspension is far easier to setup than a similar multi-link suspension and also cost less and less complex to design and manufacture [17]. With these factors in mind, it is very likely that every Formula Student team have chosen a-arm suspension design.

A-arm suspension is designed by connecting the upright to the chassis of the car. The connection links in a pair with shape of a letter A or wishbone. At the end of the link there is different type of bearings, which act as a suspension pivot point [18]. The bearings that were used for this car are rod ends connected to the chassis side and radial spherical plain bearing connected to the upright.

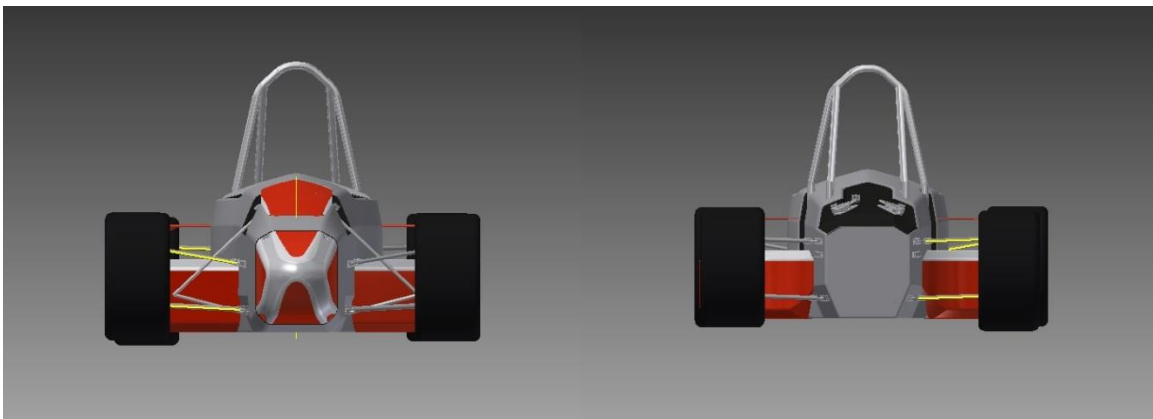


Figure 14: Front and rear right a-arm (yellow)

The length of different a-arms varies. Due to the fact that the chassis is wider at the middle section than the lower section, this allows the upper a-arm to be shorter than the lower ones. This design has a positive effect of increasing negative camber angle during upward suspension movement. The camber angle will be discussed later in Chapter 6.2. Dimension and geometry of each a-arm is shown in Table 9 below.

Table 9: A-arm dimensions and geometries

	Front		Rear	
	Upper	Lower	Upper	Lower
Length (f, r) [mm]	313, 305	350, 340	280, 260	300, 303
Angle (α) [°]	52	45	55	50
Angle to the ground (β) [°]	12.6	2	1	1

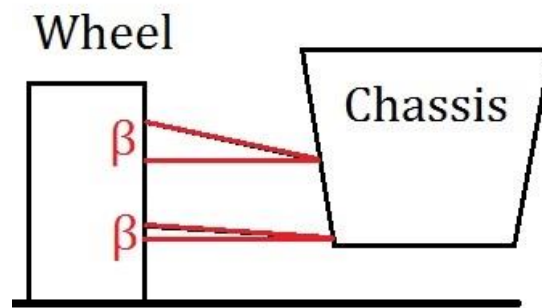


Figure 15: Upper and lower A-arm angle (β) horizontal to the ground

A-arms are mirroring each other at left and right side of the car. Length of each a-arm has been design to give 1290 mm front and 1240 mm rear wheelbase. Angle of each a-arm has been design to spread load from the wheel to the chassis as much as possible. Angle of front a-arms is limited due to conflicting with steering arm when the front wheels are turning. Angle of rear a-arms is limited due to length of the chassis and sidepods location. Horizontal angles are carefully design to let the car have best possible suspension properties i.e. roll center and camber angle gain at the front wheels which will be discussed in Chapter 6. At the rear wheels the horizontal angles are limited due to large electric motor casing blocking the way. Material used for a-arm is 4130 steel due to better mechanical properties than S355 steel, see Appendix A.1 for material properties of each alloys.



Figure 16: A-arm angle (α) with bearing housing and bearing

5.2 Push-rod

5.2.1 Push-rod and pull-rod

A-arm is designed to transfer some load from the wheel to the chassis. To transfer the force from vertical wheel travel to damper and spring components a push-rod or pull-rod has to be implemented. For push-rod, the rod reacts to the force as a compression member for a car to maintain contact with the ground while the a-arm that push-rod attaches to is reacting as a tension member. Pull-rod is the opposite of the push-rod, where the rod itself reacts as a tension member and the arm that pull-rod attaches to is reacting as a compression member [19]. Push-rod is usually attaches to lower a-arm while pull-rod attaches to upper a-arm. In this case, the suspension arm that the rod is attaches to have to be thicker and stronger.

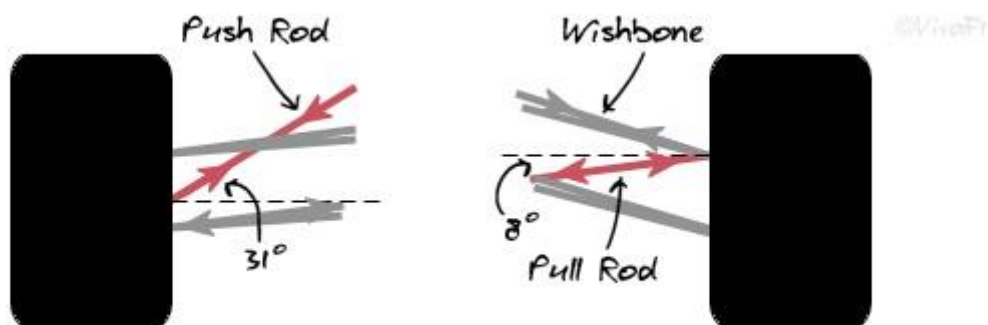


Figure 17: Push-rod vs pull-rod configuration

Image courtesy of vivaf1 (2012)

From design point of view both push-rod design and pull-rod design have advantages and disadvantages [20]:

Table 10: Push-rod and pull-rod comparison

	Advantages	Disadvantages
Push-rod	Aerodynamic benefits due to geometry Maintain the car at the same level Better load angle to the horizontal plane	Higher CoG Higher load on lower a-arm
Pull-rod	Lower CoG Easier to mount to heavy unit, which locates at the bottom of the car	Higher load on upper a-arm Aerodynamic disadvantages (at the front)

5.2.2 Load through push-rod

Push-rod is generally chosen for Formula Student car mostly due to better load angle. Load angle is much more important than losing a few milliseconds in corners and straight line aerodynamic drag. Reliability of the car is one of the most important design and engineering criteria to meet. Every year several teams have disqualified from brake test and endurance event due to failure at the joint between a-arm and push/pull rod.

Loading on push/pull rod is a function of its angle meaning that the force will be amplified from the wheel load.

$$F_{Pushrod} = \frac{F_N}{\sin(\text{angle})} \quad (11)$$

Push-rod connection point is not located at the tip of the a-arm. In this case, a 30 mm distance will be used to calculate actual push-rod force. Distance from push-rod connection point to the chassis is approximately 300 mm at the front and 280 mm at the rear.

$$F_{Pushrod,actual} = \frac{F_{pushrod} \times (30 + x)}{x} \quad (12)$$

Where: x Distance from push-rod connection point to the chassis

Table 11: Force through push-rod

	Normal force [N]	Angle [°]	Push-rod force [N]	Actual force [N]	With SF [N]
Front	1347.45	35	2349.21	2584.13	3876.19
Rear	1277.46	17	4369.32	4837.46	7256.18

Table 11 shows that push-rod force has been increased significantly from normal force. Normal force at the front wheel is largest at 1.6g cornering while at the rear wheel the force is largest at 1.1g acceleration as mentioned in Chapter 4.2 and 4.3. Push-rod force is greater at rear wheel due to much lower angle to the horizontal plane. From engineering point of view, it is desirable to have as steep push-rod angle as possible. Due to design complication between front rocker and monocoque top cover at the front and 210 mm rear wheel mount electric motor at the back, the best possible angle with 25.4 mm wheel bounce is 35 and 17 respectively.

5.2.3 Push-rod design capacity

There are 4 tube sizes available for the team during manufacturing of push-rod. However, only 2 sizes will be considered. Push-rod calculations will be based on the tube buckling capacity from Eurocode 3 in Appendix C.

Table 12: Push-rod tube dimension

Dimensions		
OD [mm]	15.88	19.05
ID [mm]	19.05	16.11
Wt [mm]	0.71	1.47
A [mm ²]	33.88	81.35

Table 13 : Input values for calculation of buckling capacity

Values	
L = L _{cr} [mm]	470 (f) & 360 (r)
F _y [MPa]	524
γ _{M1}	1.05
α	0.49

Table 14: Output for buckling capacity

	Output			
	15.88x0.71		19.05x1.47	
Length [mm]	470.00	360.00	470.00	360.00
ε	0.67	0.67	0.67	0.67
λ ₁	62.88	62.88	62.88	62.88
λ	1.39	1.10	1.20	0.92
Φ	1.76	1.28	1.46	1.10
χ	0.35	0.50	0.43	0.59
N _{b,Rd} [N]	5951.00	8492.31	17638.00	23903.33
SF	2.30	1.76	6.83	4.94

Table 14 shows that 15.88x0.71 tube has sufficient buckling capacity for both front push-rod and rear push-rod with minimum SF of 1.76 for rear push-rod.

5.3 Rocker

A rocker is a part of a suspension system where bump force is translates from push-rod into the damper and ARB by changing a linear motion of an angle. The relationships between the spring travel and wheel travel is called motion ratio. The FSAE rule for 2014 required that the car must have usable wheel travel of at least 1 inch (25.4 mm) rebound and at least 1 inch (25.4 mm) jounce with driver seated inside the vehicle [3].

$$MR = \frac{\text{Suspension travel}}{\text{Wheel travel}} \quad (13)$$

There are slightly different motion ratios between front and rear rocker. Motion ratio is measured from suspension connection point to pivot point and pushrod connection point to pivot point. Table 15 shows different length of each rocker arm motion ratio.

Table 15: Motion ratio of front and rear rocker

	Front	Rear
Suspension side [mm]	90.95	89.15
Pushrod side [mm]	55.50	57.75
Ratio	1.64	1.54

The motion ratio of front rocker is slightly higher than the rear due to high amount of unsprung mass at rear wheels. In case of hitting cones or bump rear wheel will bounce more, given that the bump force have the same magnitude.

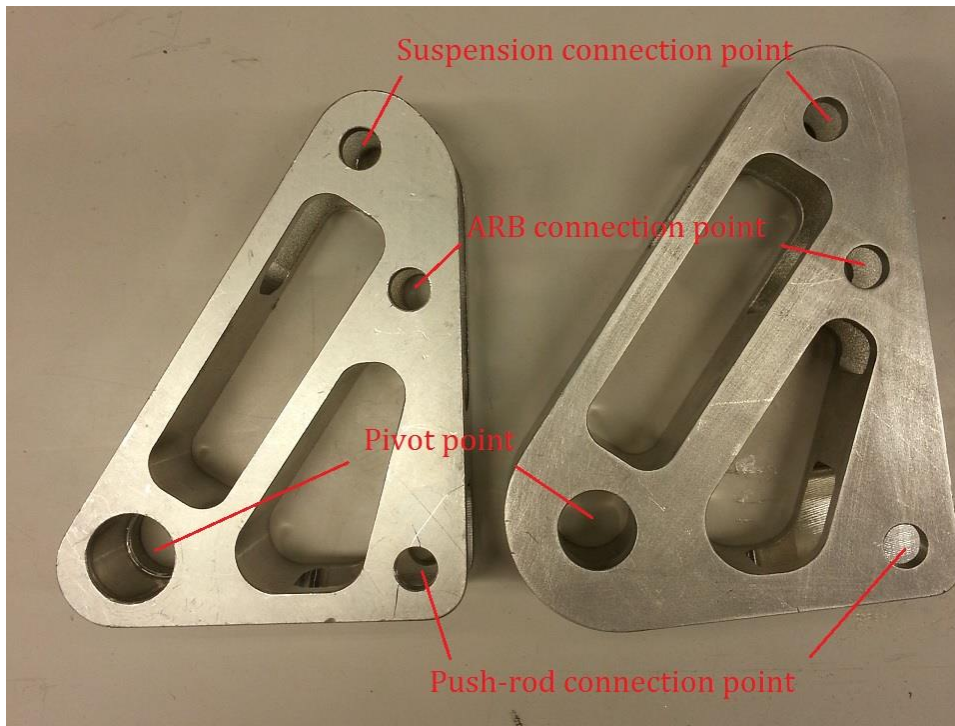


Figure 18: Front and rear rocker

Figure 18 shows front and rear rocker design. Both designs have total thickness of 26 mm with 4 mm wall thickness. The material used for rockers is 6061 T6 Aluminum alloy due to relatively high yield and tensile strength. Appendix A.2 shows the specification of 6061 T6 Aluminum. The improvement of this year rocker design is weight reduction. Weight was reduced by approximately 15% compared to the previous year.

5.4 Spring and damper

The most common type of spring is helical-coil spring. When compressed, the reaction force is developed opposite of the applied force and tries to bring the compressed spring back to its original state [21]. The damper unit is necessary to limit the amplitude of vibration. The amplitude of vibration is large near resonance. By changing the natural frequency of the system, the resonance may be avoided. Even though most springs have linear force-deflection relation when undergo small deflection, the system as a whole

has to be treated as non-linear spring. The reason involves the non-linear force-deflection relationships of the slick tires which also act as a spring system.

To reduce costs of 2014 car, springs and dampers will be taken from previous year car. The damper which has been chosen is Öhlins TTX 25. Each unit has a stroke length of 57 mm and weight approximately 448 g without spring. The springs available at the workshop range from 150 lb/in (2.68 kg/mm) to 450 lb/in (8.04 kg/mm).



Figure 19: Öhlins TTX 25 damper with spring

Image courtesy of ohlinusa (2013)

For 2013 car, the spring rate of 350 lb/in (6.25 kg/mm) has been used for both front and rear suspensions. Some testing at a closed track revealed that the inner rear wheel lift slightly during tight corner. The car also slightly understeers while cornering. To counter these issues, the same spring rate will be used at the front suspension while stiffer spring rate will be used at the rear.

5.5 Anti-roll bar

The anti-roll bar is a crucial part of the suspension system. The ARB is a torsional rod designed to resist the body roll during lateral acceleration. The concept of the ARB is to transfer some of the vertical forces from the outer wheel during the corner to inner wheels. Load transfer helps inner wheels to stick to the ground and keep the vehicle parallel to the surface [22]. Both front and rear ARB are located on top of the chassis. At the front end, there will be a thin carbon fiber cover to help direct the airflow more smoothly through the front of the car. The ARB for 2014 car will be designed as a short blade-shape [23]. The front location of the ARB for 2014 car is similar to 2012 car.

Figure 20 shows the short blade-shape design of this year ARB design. The total length is no more than 20 cm and the blade-shape design makes the stiffness of the ARB adjustable by turning the blade vertically or horizontally. The team has one dedicated student to design and analyzed the ARB for 2014 car. For this reason, the ARB part of the suspension will not be included in this thesis.



Figure 20: Anti-roll bar designed by M. Åsland.

5.6 Chapter summary

Suspension components are critical part of a race car. Each component has to be able to withstand load or transfer the load correctly so that no particular part is subject to excessive load. The a-arm or double wishbone arm is design to transfer the load to the chassis as well as provide negative camber gain during upward wheel travel.

Push-rod is designed to transfer normal force through the motion of the rocker and into the spring and damper. The force through push-rod is much lower at the front than the rear due to steeper push-rod angle at the front. The steel tube used for push-rod will be able to withstand at least 1.76 times of the maximum load through the rear push-rod and nearly 2.5 times the maximum load through front push-rod.

The relationships between suspension travel and wheel travel is called motion ratio. The motion ratio of the rocker has been increased and the rear springs have been stiffer to compensate the increase unsprung mass of the rear wheel. The adjustable blade-shaped design of ARB also provides extra stiffness and reduces the car roll while cornering.

6. Suspension properties and simulations

6.1 Introduction

Suspension properties are dynamic system. It is both difficult and time consuming to do manual calculations and interpolations to find the output for the ideal suspension setup. In this chapter ADAMS/Car and ADAMS/Solver will be used. Input for different types of simulations can be found in Appendix B, which covers parallel wheel travel, opposite wheel travel and constant corner analysis.

6.2 Roll center

6.2.1 Determining roll center

Roll center of the car is the point where during cornering the car will roll around. The point is imaginary and can be found by looking the geometry of a-arm at the front end and rear end of the car. When taken vehicle CoG into consideration, the roll center of the vehicle determines the body roll of the car [24]. If the roll center is located at the CoG, all weight transfer will go through upper and lower a-arm. However, if the roll center is located outside of the CoG location, a moment arm is create, the weight will also be transfer through springs and dampers and will cause chassis roll.

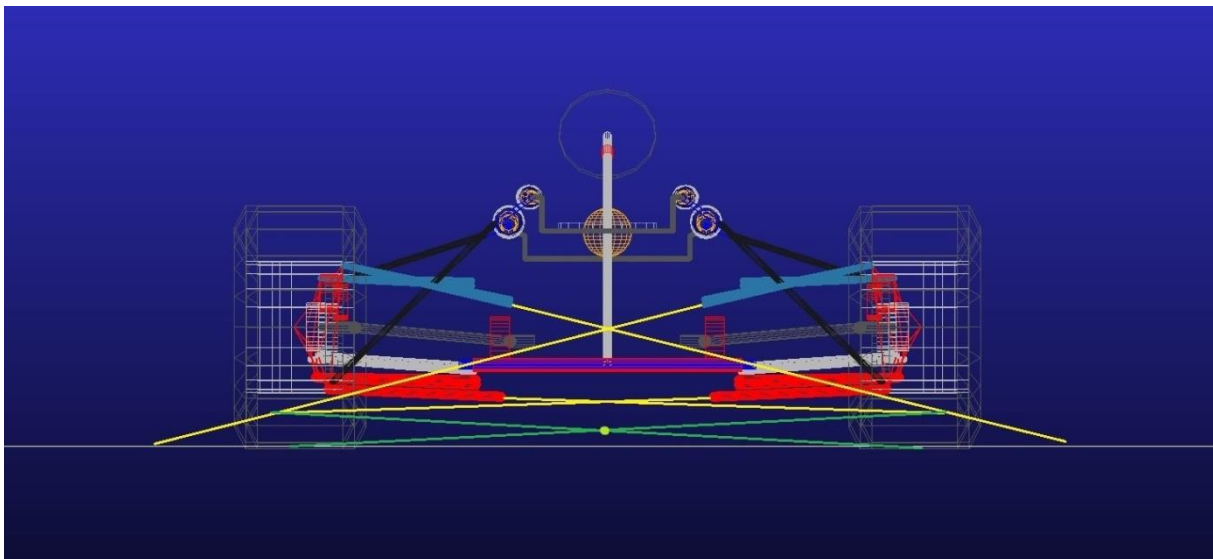


Figure 21: Front view suspension roll center

Figure 12 shows roll center of the vehicle. Roll center can be found by draw a line parallel to upper and lower a-arm (yellow). Draw another line at the point where upper and lower a-arm line intersects to the center of the wheel contacting the ground (dark green). The point where dark green lines intersect is the roll center location (light green).

6.2.2 Roll center movement

Roll center of the vehicle is not static. It will move both vertically and laterally depending on movement of the car.

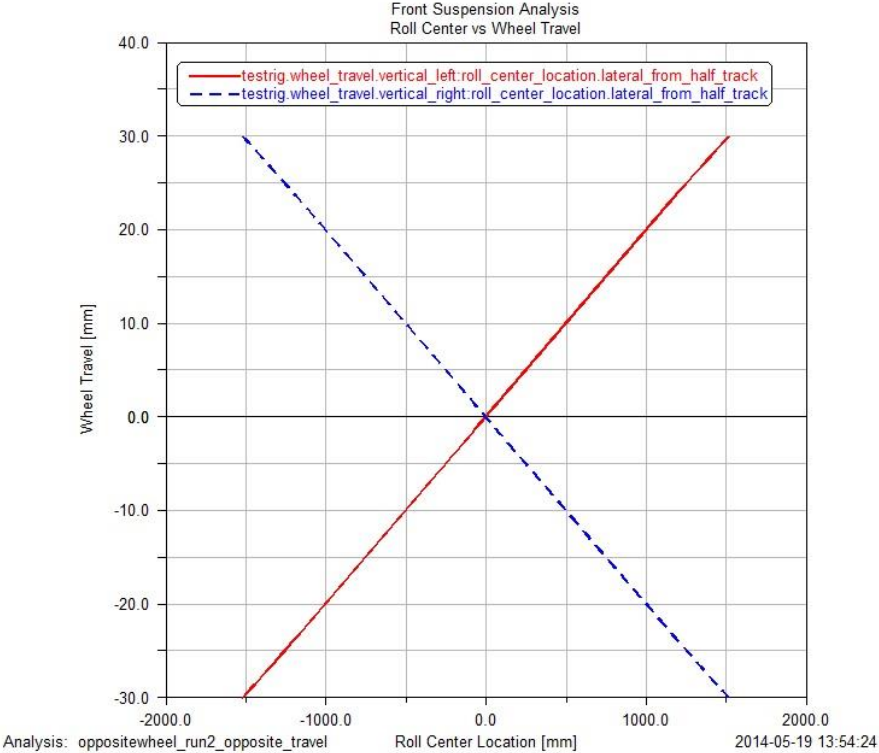


Figure 22: Front suspension lateral roll center

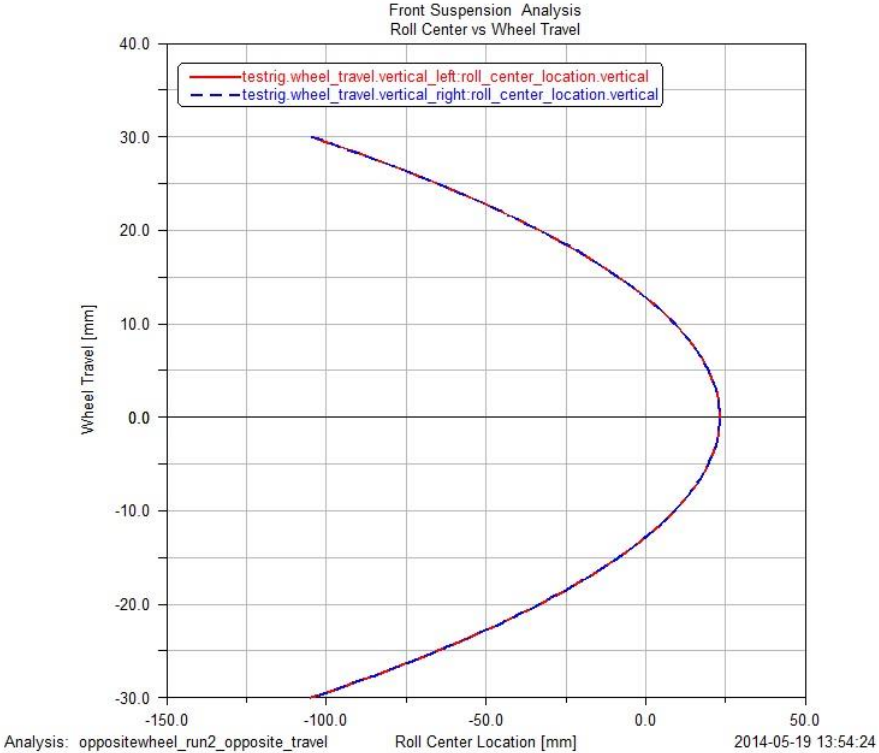


Figure 23: Front suspension vertical roll center

Figure 22 shows lateral roll center of the front suspension. The simulation is taken into account of the extreme case of linear opposite wheel travel, which explains why the graph is linear. The right wheel, represented by the blue dotted line, jounce while the left wheel, represented by the red line, bounce. At static condition the blue line and red line intersect each other at origo. This explains the static location of the roll center which is in the middle between left and right wheel. The lateral roll center of this scenario shifts as much as 1250 mm to the side when subjected to the FSAE regulation of 25.4 mm wheel travel requirement.

When the car is in equilibrium, the vertical roll center is around 25 mm above ground for front suspension, as shown in Figure 23. When subjected to wheel travel of 25.4 mm the variation of vertical roll center can be as low as -70 mm below the ground. Roll center movement will not intersect the CoG, which is approximately 300 mm above ground. In this case, the weight transfer will also go through springs and dampers as well as upper and lower a-arm.

6.2 Camber

Camber angle is defined as vertical angle of the wheel viewed from the front or the rear of the car. For race car the top of the wheel leans toward the chassis, which gives negative camber. The opposite is when the bottom part of the wheel leans toward the chassis, this is called positive camber. Slight negative camber is desired. During cornering, a negative camber helps maximize the contact between tires and the ground. For maximum cornering a negative camber angle of 0.5° is desired due to tire elastic deformation [25]. With this statement in mind every race car, under static condition, must have a negative camber at the front wheel. Disadvantages of negative camber angle are increased tire wear on the inside and reduced tire contact to the ground during the straight line driving.

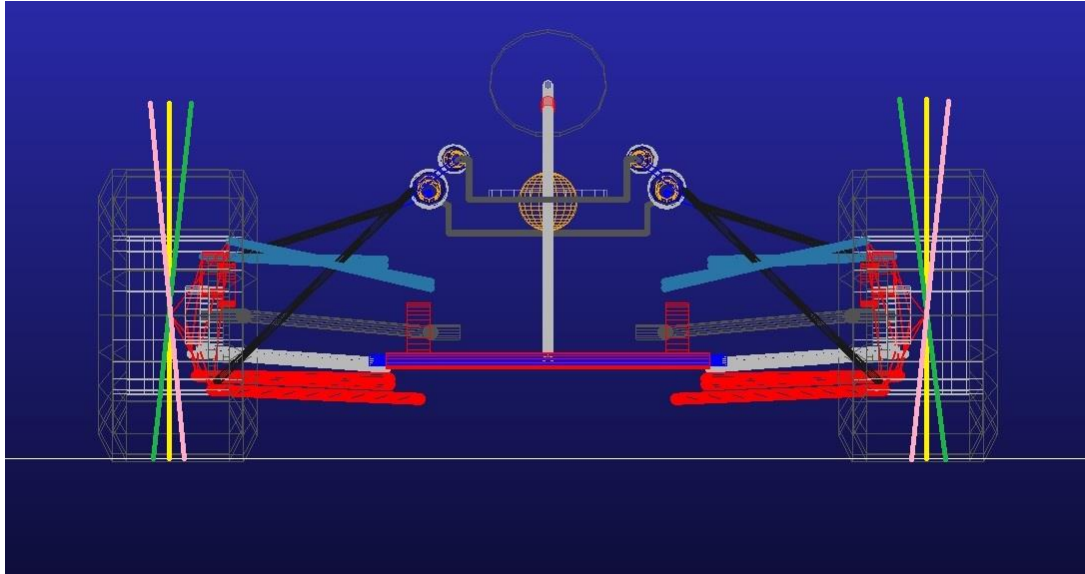


Figure 24: Camber angle at front wheel

Figure 24 shows different camber angle line for front suspension of the FS car. Yellow lines represent zero camber, green lines represent negative camber and pink lines represent positive camber.

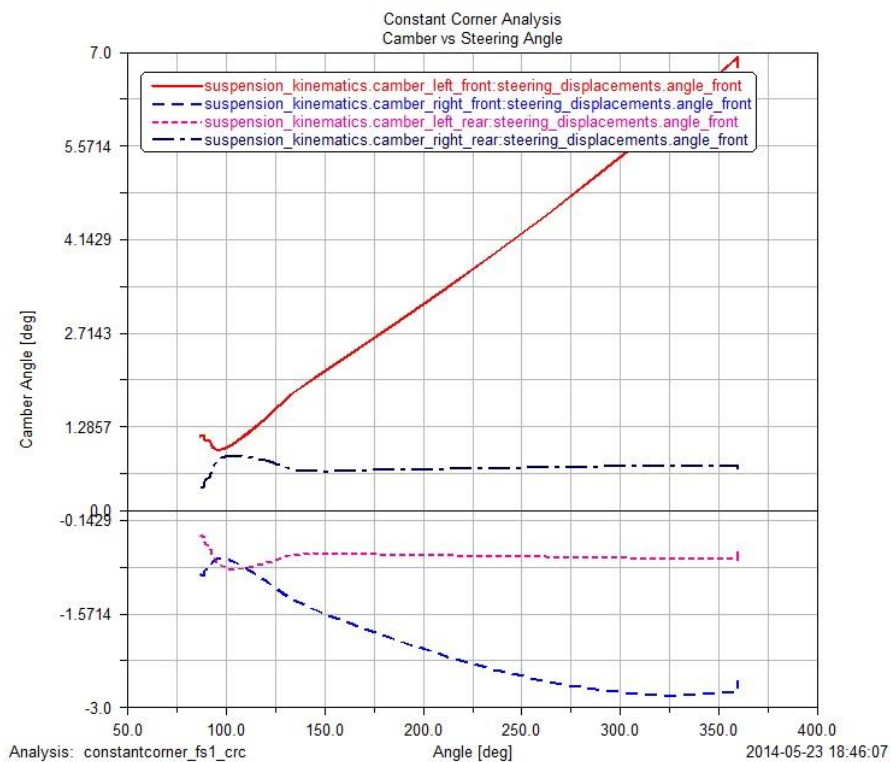


Figure 25: Camber during constant corner simulation

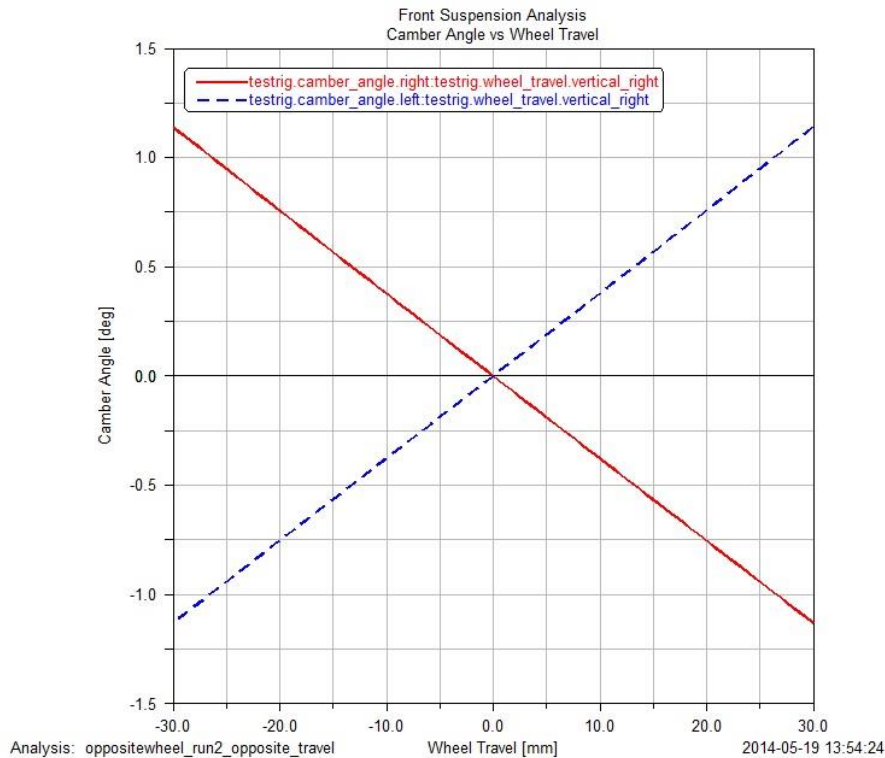


Figure 26: Front camber during opposite wheel travel

Analysis from ADAMS/Car shows that during 1.6 g constant cornering the positive camber of the front wheel could be as high as 2° at the left front wheel represented by the red line, given that the car maximum steering angle is 150° as shown in Figure 25. For rear wheel the positive camber angle could theoretically be around 0.7° at the maximum as shown by the black dotted line. Higher camber at the front wheel is due to steeper a-arm angle to the horizontal plane. The front wheel also has more vertical movement due to the effect of centrifugal force as discussed in Chapter 4.2. The negative camber gain of -1.5° is desirable at the right front wheel (blue dotted line) to increase the contact between the tire and the ground.

For opposite wheel travel simulation, the positive camber is just below 1° as shown in Figure 26. The negative camber is also right below 1° for both right and left wheel, as illustrate by red and blue dotted line respectively. It is clear that constant corner simulation shows more positive camber gain. In this case, the setup of the car should be done by using the result from Figure 25.

Both simulations are based on 0 camber angle under static condition. When setting up the car in reality, the camber should be 2° before skid-pad event and around 1° at other events. Static camber should be 0° during acceleration event.

Positive camber angle is undesired for a race car point of view and should not be setup under static condition.

6.3 Caster angle

Caster angle is best described as the vertical angle of steering pivot axis view from the side of the car. The pivot can tilt backward, neutral and forward. Positive caster has backward tilt, which means the top pivot pointing toward the rear of the car and opposite for forward tilt. Figure 27 shows positive caster angle (green) viewing from the left side of the car.

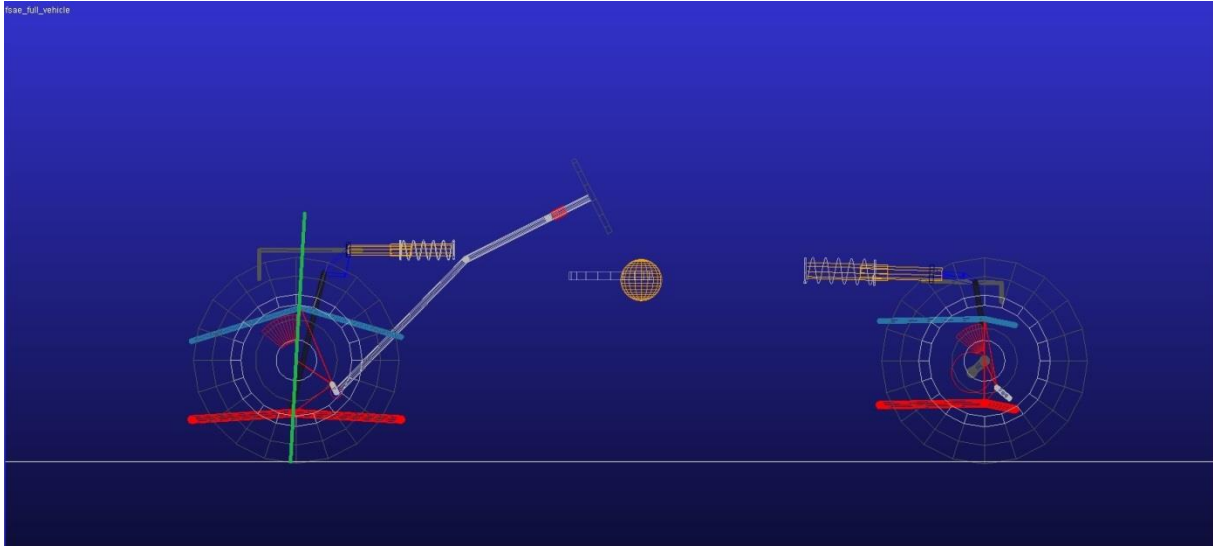


Figure 27: Left view of the car with positive front caster

This year car is designed to have around 5° positive caster at the front wheel and neutral caster at the rear. Positive caster cause steering axis to point toward the ground at the front of tire contact patch. When the car accelerates positive caster helps to create a self-centering effect to enhance straight line stability. Another positive effect of caster is the slight camber change during cornering. The inside wheel will slightly gains positive camber and outside wheel will slightly gains negative camber. The negative effect of caster is slightly heavier steering effort.

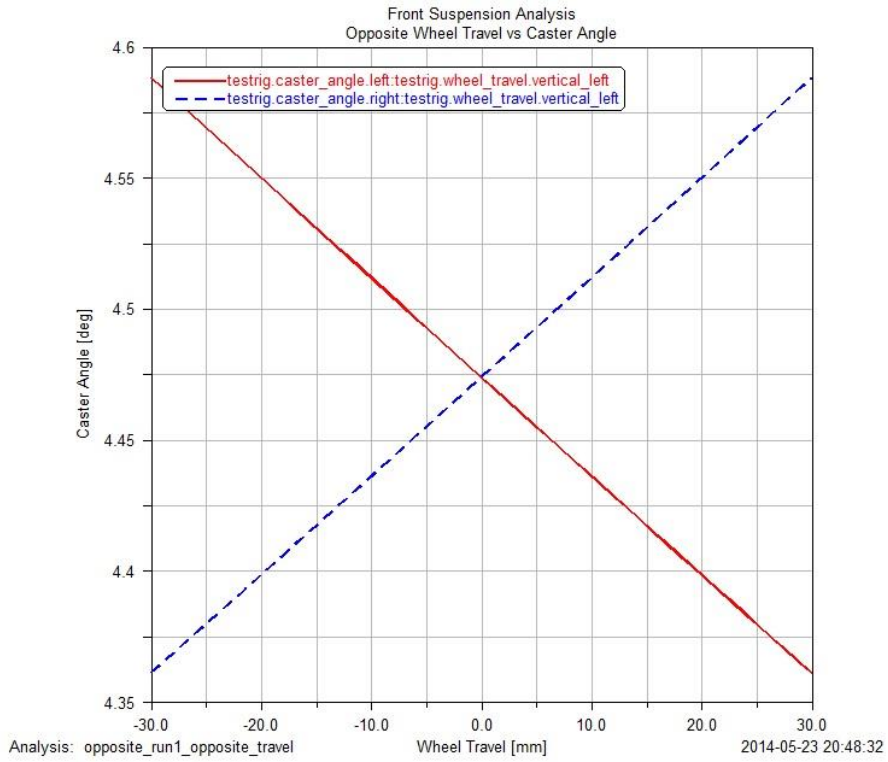


Figure 28: Front caster of opposite wheel travel

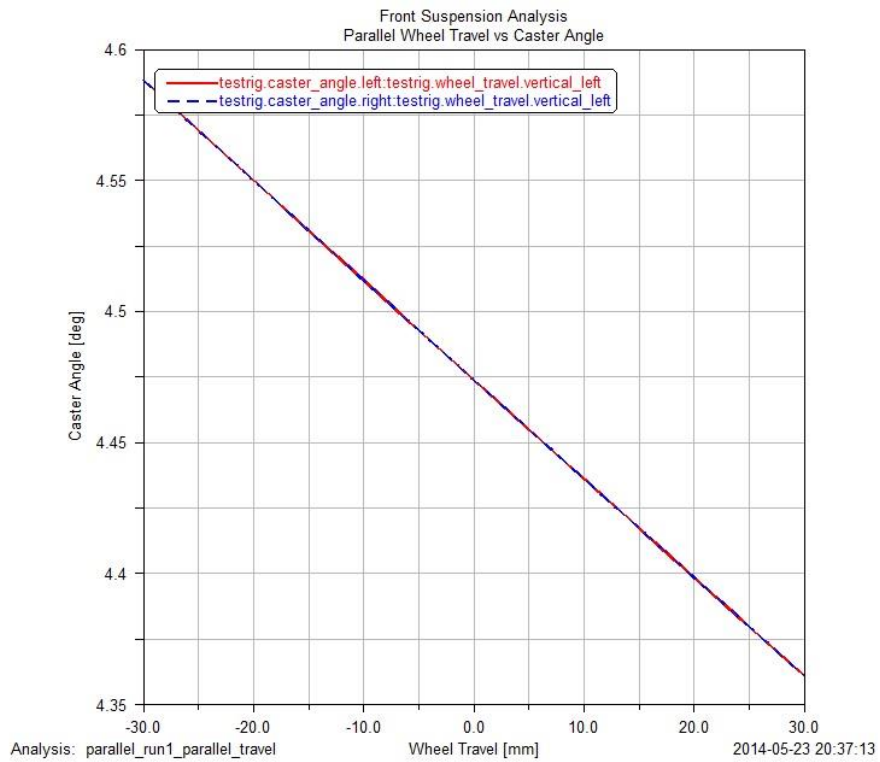


Figure 29: Front caster during parallel wheel travel

Figure 28 and 29 shows the postprocessor from ADAMS/Car. Both figures show that the actual designed caster angle is 4.475° . The caster angle is the same for left and right wheel, as illustrated by red and blue dotted line respectively. For both opposite wheel travel and parallel wheel travel of 25.4 mm, the caster changed only $\pm 0.1^\circ$. These values are desirable due to caster change is minimal and within the area of $3-5^\circ$.

6.4 Toe

Toe angle is the angle of the wheel, seen from the top of the car. Zero-toe is when this angle makes both wheels pointing parallel and straight forward. Toe-out is when the wheel pointing away of the car, opposite for toe-in.

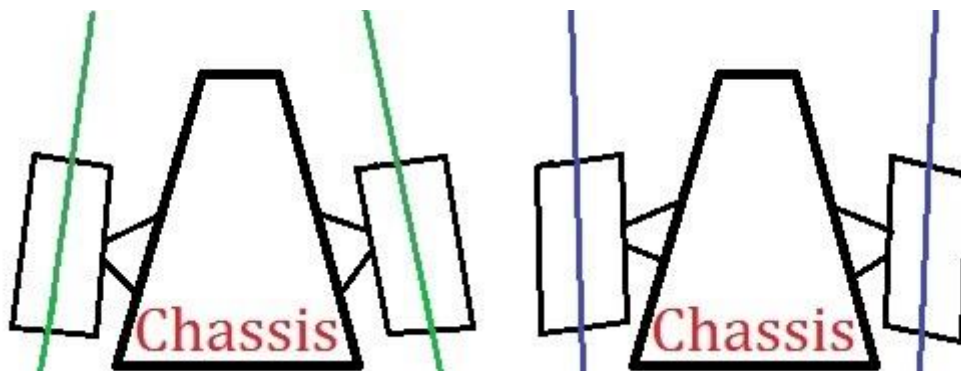


Figure 30: Illustration of toe-in and toe-out

Figure 30 shows the toe angle difference between toe-in (green) and toe-out (blue). Toe-out setup causes the car to be more sensitive to disturbance. When a car entering a turn with slight disturbance, it will give better feedback due the car will be trying to enter a turn. Toe-in setup of a car act as a complete opposite. Slight disturbance will not enhance the car feedback. In this regard, toe-in increase straight line stability of the car, while toe-out improves cornering ability. A drawback of toe-in and toe-out is increase tire wear.

The 2014 car will be able to adjust both front and rear toe angle. At the front, the toe angle will be adjusted by turning the steering arm while at the rear the toe angle will be adjusted by turning the toe-rod. The rear wheel of the car will have 0 toe angle configuration. At the front wheel toe-in configuration will be used at the acceleration event due to improve stability for high speed driving in straight line. Toe-out configuration will be used during all other events.

6.4.1 Bump steer

Bump steer can be easily explained by upward parallel wheel travel. Bump steer is undesirable for the race car due to bumps can cause more toe out than necessary and can cause a car to travel to an unintended direction.

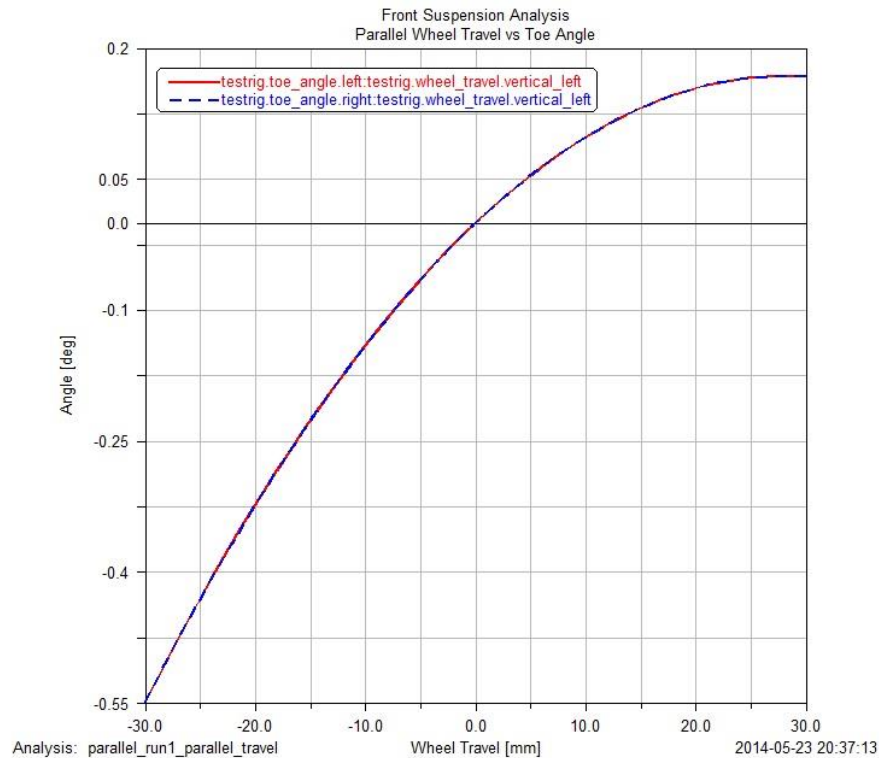


Figure 31: Bump steer caused by parallel wheel travel

The 2014 car is designed to be able to handle slight bump steer caused by bump in race tracks. The simulation shows that under static condition the car have 0 toe and toe will not exceed 0.2° at 25.4 mm parallel wheel travel. If the car is setup properly, the toe angle of left and right wheel should be exactly the same, as shown in Figure 31 by red and blue dotted line respectively. However, when building the car for the race events (beside acceleration event) the car will have around 0.2° to 0.5° toe-out to enhance cornering ability of the car. At Silverstone racetrack, the track is relatively flat and 25.4 mm of parallel wheel travel will be highly unlikely to occur.

6.4.2 Roll steer

Roll steer is similar to bump steer. The main different is for roll steer 1 wheel will rise while the other will fall. Unlike bump steer, roll steer does not measured in degrees but in degrees of toe per degrees of roll.

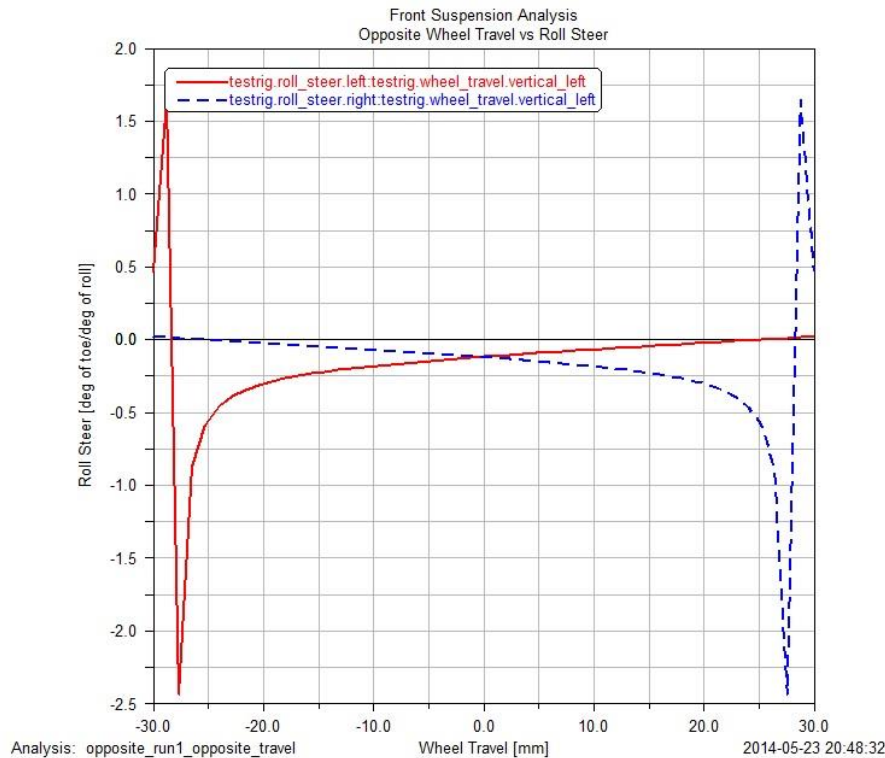


Figure 32: Roll steer caused by opposite wheel travel

Roll steer will more likely to occurs at the racetrack than bump steer. When the car is moving with relatively high lateral acceleration around the corner the inner wheel will drop while the outer wheel will rise and the suspension will compress. This effect can be similar to roll steer. Simulation shows that for maximum wheel travel for roll steer is between -0.5 to 0 most of the time. However, if both wheel movements are greater than 50 mm the roll steer will greatly increase to nearly -2.5. These results mean that roll steer will slightly cause toe-in which gives a negative handling effect during the race. Sudden changes in roll steer at 28 mm wheel travel may due to simulation error and should be neglected.

6.5 Scrub radius

Scrub radius is an important aspect of the steering of the car. Scrub radius can be easily explained as the distance between the centerline of the tire contact patch to the line between upper and lower control arm pivot point extended to intersect the ground [26], shown by yellow line in Figure 22 below. The angle between the extended line of upper and lower control arm pivot point and vertical line at the center of the tire is called kingpin inclination angle. Scrub radius is zero when these two lines intersect at the center of the tire contact patch. Positive scrub is when intersection point is below the road surface and opposite for negative scrub.

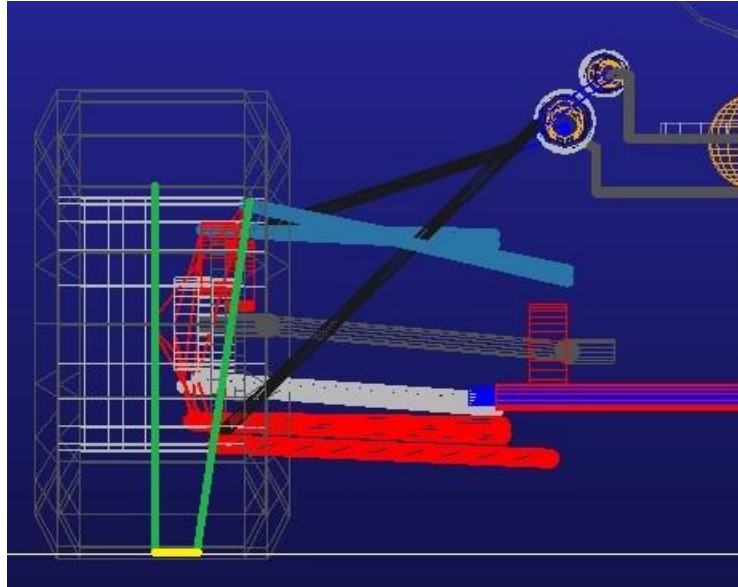


Figure 33: Front view scrub radius

The design of this year formula car will aim to have scrub radius between 40-60 mm and kingpin inclination angle of around 5°. The reason for this is to have sufficient scrub to provide turning moment when the wheels are rotate while moving due to increase in front tires contact patch. For rear wheel drive, this effect will also cause the wheel to slightly toe-out and improve handling [27]. The drawback of excessive amount of scrub is heavier handling.

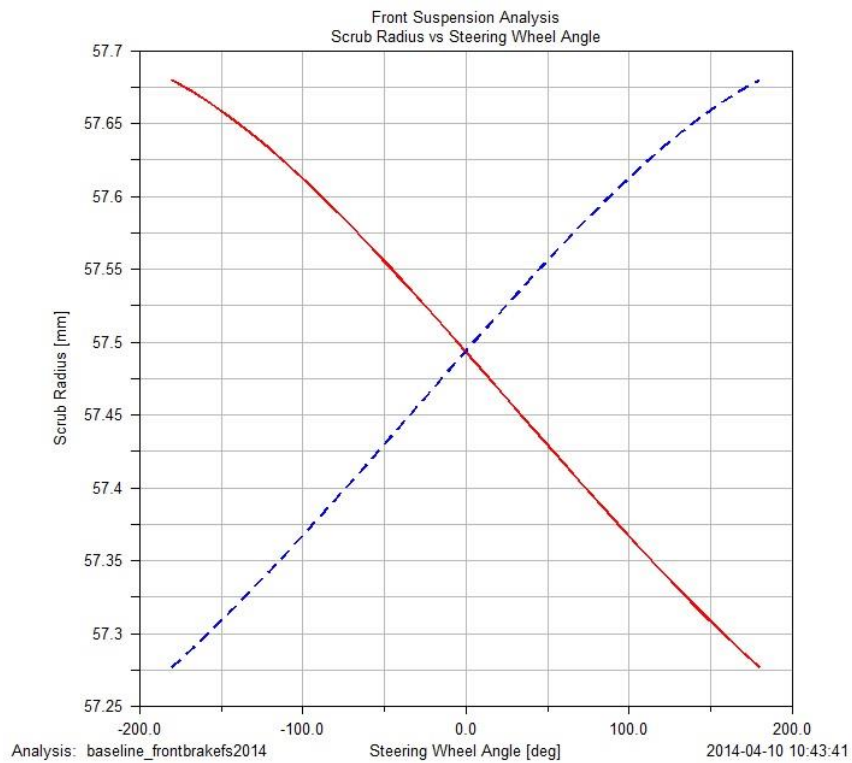


Figure 34: Change in scrub radius when steering angle change

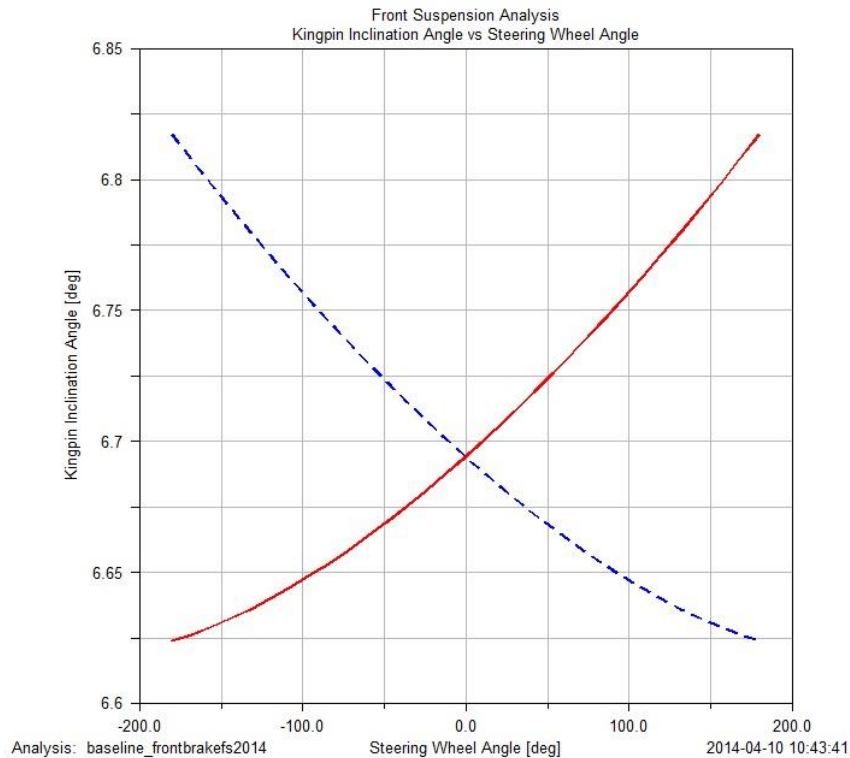


Figure 35: Change in kingpin inclination angle with different steering angle

Simulation shows that the designed scrub radius is approximately 57.5 mm and will change by less than 0.3 mm (assuming maximum steering angle is 150°) as shown in Figure 34. The scrub radius is identical at left and right wheel as illustrate by red and blue dotted line. Kingpin inclination angle is approximately 6.7° and have less than 0.1° degree change as shown in Figure 35. The result has proven that the a-arm pivot point could have been designed better.

It is however more desirable to have scrub radius toward 40 mm than 60 mm, but due to the gap between wheel hub and upright, upright design and upright bracket, it is not possible to have less than 57,5 mm scrub radius. With this result, it is not possible to have 5° kingpin inclination as aimed otherwise the scrub radius will be larger, which will results in heavier steering for the driver.

6.6 Chapter summary

Proper suspension properties help to improve dynamic of the race car. The location of roll center of the car determines the weight transfer and the car roll. If the roll center is at the exact location of CoG then the car will not roll and all weight will transfer through upper and lower a-arm. Otherwise weight transfer will goes through springs and dampers. Location of roll center and movement of roll center during wheel travel is depending on a-arm geometry. Vertical roll center movement can varies by few centimeters while horizontal roll center movement can varies by up to several meters.

Slightly negative camber angle helps to improve the contact between the tires and the ground. Negative camber angle of 2° helps to prevent the angle to become positive

during vertical wheel travel. Positive camber angle has no positive effect for track car and should be avoided. Caster angle should be slightly positive. Positive caster has backward tilt. At around 5° of caster will enhance the car straight line ability and also affect the outside wheel to slightly gain negative camber during cornering.

Toe-out configuration will give extra feedback to the driver when the car trying to enter a turn. The opposite occurs for toe-in. Any events with left or right turns, the car should have toe-out configuration. Toe angle can also be affected by bump steer and roll steer.

Scrub radius is the distance between the centerline of tire contact patch and the line between the upper and lower a-arm pivot point, extended to the ground. The distance creates extra front tires contact patch and will provide turning moment when the wheels are rotating while moving. Scrub radius around 40 mm is preferred. Too much scrub results in heavier steering.

7. Conclusion and future work

7.1 Conclusion

The suspension design of this year car was done with the goal to reduce weight, improve load distribution and improve handling characteristics of the car. Due to relatively wide vehicle track and relatively long wheelbase compared to top teams, it is decided at these 2 parameters will stay the same as previous year. Sprung mass at the front suspension has been reduced by over 30%, while unsprung mass is increased by 2%. While at the rear suspension the sprung mass has been reduced by nearly 30% while unsprung mass has been increased by double due to electric engine and gear mounted at the rear wheel.

The suspension has been designed to handle the same amount of g-force as achieved from the vehicle from top teams. The actual force through push-rod could be up to nearly 5 kN at the rear, twice as much as the force through front push-rod due to steeper angle at the front. There are safety factor of 2.3 and 1.76 respectively to handle the force through push-rod. At the same time, motion ratio of the rocker have been increased as well as spring stiffness at rear suspension to handle the increased rear unsprung mass of the car.

ADAMS/Car simulation and manual calculations revealed that outer front wheel has largest lateral force in corner while rear wheel have largest longitudinal force from acceleration. Wheel movement simulation of 30 mm and steering wheel angle simulation also shows that different suspension properties are mostly within design goal such as low camber, caster and toe angle change. Most of these properties changed within 1° from the static condition. The only simulation that shows significant deviation compared to design goal is kingpin inclination angle. The aim to have less than 60 mm scrub radius means that kingpin inclination angle has to be 6.7° , 1.3° more than expected. Most of the simulations have been done while the car is at static condition. In this case, the suspension setup can be tuned according to the simulation results to meet the requirement. Overall, the suspension system is proven to be properly designed.

7.2 Future work

There has been done a thorough work of suspension analysis of this year car. However, there are some potential improvements in design aspect as well as additional simulation parameters to be done in the future, such as:

- Investigate the possibility to use carbon fiber instead of steel tubes at a-arm and push/pull-rod. Weight reduction will be even more significant.
- Possibility to design a pull-rod system to achieve lower CoG.
- Move electric engine inside the chassis to decrease unsprung mass. This will also open the possibility to increase the push-rod angle at the rear and lower the force through push-rod.
- Add the tire stiffness of the Hoosier tires into ADAMS/Car simulation.

References

- [1] J. L. Ortiz, "Introduction to Adams / Solver C ++," 2011. [Online]. Available: <http://pages.mscsoftware.com/rs/mscsoftware/images/AdamsUserMeeting-IntroductioSolver.pdf>. [Accessed: 21-Mar-2014].
- [2] I. Aguinaga, "Multi-body Systems," 2012. [Online]. Available: <http://www.unav.es/adi/UserFiles/File/4000005502/6.Multibody.pdf>. [Accessed: 21-Mar-2014].
- [3] SAE, "2014 Formula SAE ® Rules." SAE International, 2014.
- [4] C. Scarborough, "Why is wheelbase important," 2010. [Online]. Available: <http://scarbsf1.com/blog1/2010/02/18/why-is-wheelbase-important/>. [Accessed: 24-Feb-2014].
- [5] A. Staniforth, *Competition car suspension - A practical handbook*, 4th ed. Sparkford, Yeovil, Somerset: Haynes Publishing, 2006.
- [6] V. Brevik, "Design, Analysis and Simulation of the Suspension System in the FS Team UiS Race Car," University of Stavanger, 2013.
- [7] A. van Berkum and T. U. Eindhoven, "Chassis and suspension design FS RTE02," Eindhoven University of Technology, 2006.
- [8] A. Mouzouris, "F1 Tires...Part 2," 2012. [Online]. Available: <http://technicalf1explained.blogspot.no/2012/10/f1-tirespart-2.html>. [Accessed: 26-Feb-2014].
- [9] P. Wright, "Formula 1 and road cars compared," 1999. [Online]. Available: <http://www.grandprix.com/ft/ft00308.html>. [Accessed: 26-Feb-2014].
- [10] SEAS, "Weight transfer." [Online]. Available: http://www.formula1-dictionary.net/weight_transfer.html. [Accessed: 03-Feb-2014].
- [11] J. W. J. Jewett and R. A. Serway, *Physics for Scientists and Engineers*, 7th ed. London: Thomson Learning, 2007, p. 84.
- [12] "Formula Student 2013," *Institution of Mechanical Engineers*, 2013. [Online]. Available: <http://www.formulastudent.com/docs/default-source/results-2013/acceleration-final-results-2013.pdf?sfvrsn=0>. [Accessed: 02-Mar-2014].
- [13] "Formula Student 2013," *Institution of Mechanical Engineers*, 2013. [Online]. Available: <http://www.formulastudent.com/docs/default-source/results-2013/skidpad-final-results-2013.pdf?sfvrsn=0>. [Accessed: 02-Mar-2014].
- [14] W. F. Milliken and D. L. Milliken, *Race Car Vehicle Dynamics, Volum 1*, 1st ed. Society of Automative Engineers, 1995.

- [15] B. M. Klebanov, D. M. Barlam, and F. E. Nystrom, *Machine Elements Life and Design*, 1st ed. Boca Raton, FL: CRC Press, 2008, p. 404.
- [16] J. Veranth, "Elements of Structures Supplemental Discussion - Safety Factors," 2013.
- [17] T. Raiciu, "How Multi-Link Suspension Works," 2009. [Online]. Available: <http://www.autoevolution.com/news/how-multi-link-suspension-works-7804.html>. [Accessed: 20-Apr-2014].
- [18] Michaeldelaney, "Double Wishbone vs. MacPherson Strut I:The Basics," 2002. [Online]. Available: <http://www.team-integra.net/forum/blogs/michaeldelaney/153-double-wishbone-vs-macpherson-strut-i-basics.html>.
- [19] Maverick, "Suspension: Pushing and Pulling," 2012. [Online]. Available: <http://www.vivaf1.com/blog/?p=10173>. [Accessed: 11-Feb-2014].
- [20] Ferlonso, "Pullrod vs Pushrod suspension: Which is preferred?," 2013. [Online]. Available: <http://www.sportskeeda.com/f1/pullrod-vs-pushrod-suspension-which-is-preferred/>. [Accessed: 05-Feb-2014].
- [21] S. S. Rao, "Mechanical Vibrations," 5th ed., Jurong: Pearson Education, 2011, pp. 22–23.
- [22] F. Danielsen, "Anti roll bar system for Formula Student car," University of Stavanger, 2012.
- [23] M. Åsland, "Design og valg av type anti roll bar for formula student bil," University of Stavanger, 2014.
- [24] SEAS, "Roll Center." [Online]. Available: http://www.formula1-dictionary.net/roll_center.html. [Accessed: 22-Mar-2014].
- [25] J. Hagerman, "Camber, Caster and Toe: What Do They Mean?" [Online]. Available: <http://www.ozebiz.com.au/racetech/theory/align.html>. [Accessed: 11-Feb-2014].
- [26] R. Jackman, "Scrub Radius." [Online]. Available: http://www.hrsprings.com/technical/scrub_radius. [Accessed: 11-Mar-2014].
- [27] I. Andrew and R. Beaumont, "Scrub Radius." [Online]. Available: <http://www.cdxetextbook.com/steersusp/wheelsTires/alignFund/scrubradius.html>. [Accessed: 11-Mar-2014].

Appendix A: Material properties

A.1 Steel

Chemical Elements (Wt%)	4130	S355
Fe	Balance	Balance
C	0.33	Max 0.23
Cr	1.1	-
Mn	0.6	Max 1.6
Mo	0.25	-
P	0.025	Max 0.05
S	0.025	Max 0.05
Si	0.35	Max 0.05
Cu	0.35	-

Mechanical Properties	4130	S355
0.2% Yield strength [MPa]	524	355
Ultimate tensile strength [MPa]	663	470

A.2 Aluminum

Chemical Elements (Wt%)	6061 T6	6082 T6
Al	95.8-98.6	95.2-98.3
Cr	0.04-0.35	Max 0.25
Cu	0.15-0.4	Max 0.1
Fe	Max 0.7	Max 0.5
Mg	0.8-1.2	0.6-1.2
Mn	Max 0.15	0.4-1.0
Si	0.4-0.8	0.7-1.3
Ti	Max 0.15	Max 0.1
Zn	Max 0.25	Max 0.2
Other, each	Max 0.05	Max 0.05
Other, total	Max 0.15	Max 0.15

Mechanical Properties	6061 T6	6082 T6
0.2% Yield strength [MPa]	276	250
Ultimate tensile strength [MPa]	310	290

Appendix B: Input for ADAMS/Car

B.1 Front suspension coordinates

Assembly		Subsystem		fsae_full_vehicle.fsae_front_susp	Name Filter: *
	loc_x	loc_y	loc_z	remarks	
hpl_BC_axis	-409.6	-254.0	333.0	(none)	
hpl_BC_center	-446.6	-234.0	364.6	(none)	
hpl_damper_inboard	-181.0	-163.2	422.7	(none)	
hpl_damper_outboard	-435.0	-153.2	422.2	(none)	
hpl_lca_front	-816.0	-219.1	11.85	(none)	
hpl_lca_outer	-572.0	-574.0	27.4	(none)	
hpl_lca_rear	-308.0	-219.1	11.85	(none)	
hpl_prod_inboard	-495.0	-234.0	367.3	(none)	
hpl_prod_outboard	-572.0	-565.0	42.4	(none)	
hpl_ride_height	-816.0	-219.1	21.85	(none)	
hpl_tierod_inner	-465.0	-304.8	77.4	(none)	
hpl_tierod_outer	-475.0	-595.0	97.4	(none)	
hpl_uca_front	-816.0	-200.05	202.0	(none)	
hpl_uca_outer	-552.0	-544.0	283.0	(none)	
hpl_uca_rear	-308.0	-200.05	212.0	(none)	
hpl_wheel_center	-562.0	-645.0	155.2	(none)	
hps_camber_adj_orient	-562.0	0.0	27.4	(none)	

Assembly		Subsystem		fsae_full_vehicle.fsae_front_arb	Name Filter: *
	loc_x	loc_y	loc_z	remarks	
hpl_arb_bend	-652.0	-135.0	353.4	(none)	
hpl_drop_link	-405.0	-155.0	422.4	(none)	
hpl_leaf_link	-652.0	-135.0	422.0	(none)	
hps_arb_center	-652.0	0.0	353.4	(none)	

B.2 Rear suspension coordinates

Assembly		Subsystem: fsae_full_vehicle.fsae_rear_susp		Name Filter: *
	loc_x	loc_y	loc_z	remarks
hpl_BC_axis	980.0	-274.0	408.0	(none)
hpl_BC_center	1055.0	-204.0	361.8	(none)
hpl_damper_inboard	675.0	-203.2	374.0	(none)
hpl_damper_outboard	1005.2	-203.2	364.0	(none)
hpl_drive_shaft_inr	1078.0	-200.66	126.06	(none)
hpl_lca_front	854.4	-271.0	46.6	(none)
hpl_lca_outer	1108.4	-600.0	51.6	(none)
hpl_lca_rear	1182.4	-271.0	36.6	(none)
hpl_prod_inboard	1086.0	-254.0	344.5	(none)
hpl_prod_outboard	1103.0	-559.8	245.6	(none)
hpl_ride_height	1078.0	-381.0	63.5	(none)
hpl_tierod_inner	1168.4	-275.6	63.5	(none)
hpl_tierod_outer	1138.4	-610.6	88.9	(none)
hpl_uca_front	854.4	-279.4	250.6	(none)
hpl_uca_outer	1108.4	-590.0	255.6	(none)
hpl_uca_rear	1182.4	-279.4	240.6	(none)
hpl_wheel_center	1108.4	-620.0	154.0	(none)
hps_camber_adj_orient	1108.4	0.0	51.6	(none)

Assembly		Subsystem: fsae_full_vehicle.fsae_rear_arb		Name Filter: *
	loc_x	loc_y	loc_z	remarks
hpl_arb_bend	1150.0	-170.0	296.4	(none)
hpl_drop_link	960.0	-180.0	348.0	(none)
hpl_leaf_link	1150.0	-170.0	343.0	(none)
hps_arb_center	1150.0	0.0	296.4	(none)

B.3 Parallel wheel travel

Suspension Analysis: Parallel Travel

Suspension Assembly: frontfs2014

Output Prefix: parallel_run1

Number of Steps: 50

Mode of Simulation: interactive

Vertical Setup Mode: Wheel Center

Bump Travel: 30

Rebound Travel: -30

Travel Relative To: Wheel Center

Control Mode: Absolute Relative

Fixed Steer Position:

Steering Input: Angle Length

Create Analysis Log File

OK Apply Cancel

B.4 Opposite wheel travel

Suspension Analysis: Opposite Travel

Suspension Assembly: frontfs2014

Output Prefix: Oppositewheel_run2

Number of Steps: 100

Mode of Simulation: interactive

Vertical Setup Mode: Wheel Center

Bump Travel: 30

Rebound Travel: -30

Travel Relative To: Wheel Center

Control Mode: Absolute Relative

Fixed Steer Position:

Steering Input: Angle Length



Coordinate System: Vehicle



Create Analysis Log File

OK Apply Cancel

B.5 Constant corner

A Full-Vehicle Analysis: Constant Radius Cornering X

Full-Vehicle Assembly	fsae_full_vehicle
Output Prefix	constantcorner_run7
Simulation Mode	interactive
Road Data File 	mdids://acar_shared/roads.tbl/2d_f
Output Step Size	0.1
Gear Position 	3
Turn Radius	8250
Length Units	model
Turn Direction	<input checked="" type="radio"/> left <input type="radio"/> right
Control	<input type="radio"/> velocity <input checked="" type="radio"/> lateral acceleration
Duration of maneuver	10
Initial Acceleration	0.5
Final Acceleration	1.6
Acceleration Units	g
<input type="checkbox"/> Shift Gears	
<input checked="" type="checkbox"/> Quasi-Static Skidpad Setup	
Entry Distance	<input type="text"/> <input type="text"/> model units
Settle Time	<input type="text"/>
<input checked="" type="checkbox"/> Create Analysis Log File	

  OK Apply Cancel

Appendix C: Eurocode 3

EN 1993-1-1: 2005 (E)

(2) The following criterion should be met:

$$\frac{N_{Ed}}{A_{eff} f_y / \gamma_{M0}} + \frac{M_{y,Ed} + N_{Ed} e_{Ny}}{W_{eff,y,min} f_y / \gamma_{M0}} + \frac{M_{z,Ed} + N_{Ed} e_{Nz}}{W_{eff,z,min} f_y / \gamma_{M0}} \leq 1 \quad (6.44)$$

where A_{eff} is the effective area of the cross-section when subjected to uniform compression

$W_{eff,min}$ is the effective section modulus (corresponding to the fibre with the maximum elastic stress) of the cross-section when subjected only to moment about the relevant axis

e_N is the shift of the relevant centroidal axis when the cross-section is subjected to compression only, see 6.2.2.5(4)

NOTE The signs of N_{Ed} , $M_{y,Ed}$, $M_{z,Ed}$ and $\Delta M_i = N_{Ed} e_{Ni}$ depend on the combination of the respective direct stresses.

6.2.10 Bending, shear and axial force

(1) Where shear and axial force are present, allowance should be made for the effect of both shear force and axial force on the resistance moment.

(2) Provided that the design value of the shear force V_{Ed} does not exceed 50% of the design plastic shear resistance $V_{pl,Rd}$ no reduction of the resistances defined for bending and axial force in 6.2.9 need be made, except where shear buckling reduces the section resistance, see EN 1993-1-5.

(3) Where V_{Ed} exceeds 50% of $V_{pl,Rd}$ the design resistance of the cross-section to combinations of moment and axial force should be calculated using a reduced yield strength

$$(1-\rho)f_y \quad (6.45)$$

for the shear area

where $\rho = (2V_{Ed} / V_{pl,Rd} - 1)^2$ and $V_{pl,Rd}$ is obtained from 6.2.6(2).

NOTE Instead of reducing the yield strength also the plate thickness of the relevant part of the cross section may be reduced.

6.3 Buckling resistance of members

6.3.1 Uniform members in compression

6.3.1.1 Buckling resistance

(1) A compression member should be verified against buckling as follows:

$$\frac{N_{Ed}}{N_{b,Rd}} \leq 1,0 \quad (6.46)$$

where N_{Ed} is the design value of the compression force;

$N_{b,Rd}$ is the design buckling resistance of the compression member.

(2) For members with non-symmetric Class 4 sections allowance should be made for the additional moment ΔM_{Ed} due to the eccentricity of the centroidal axis of the effective section, see also 6.2.2.5(4), and the interaction should be carried out to 6.3.4 or 6.3.3.

- (3) The design buckling resistance of a compression member should be taken as:

$$N_{b,Rd} = \frac{\chi A f_y}{\gamma_{M1}} \quad \text{for Class 1, 2 and 3 cross-sections} \quad (6.47)$$

$$N_{b,Rd} = \frac{\chi A_{eff} f_y}{\gamma_{M1}} \quad \text{for Class 4 cross-sections} \quad (6.48)$$

where χ is the reduction factor for the relevant buckling mode.

NOTE For determining the buckling resistance of members with tapered sections along the member or for non-uniform distribution of the compression force second order analysis according to 5.3.4(2) may be performed. For out-of-plane buckling see also 6.3.4.

- (4) In determining A and A_{eff} holes for fasteners at the column ends need not to be taken into account.

6.3.1.2 Buckling curves

- (1) For axial compression in members the value of χ for the appropriate non-dimensional slenderness $\bar{\lambda}$ should be determined from the relevant buckling curve according to:

$$\chi = \frac{1}{\Phi + \sqrt{\Phi^2 - \bar{\lambda}^2}} \quad \text{but } \chi \leq 1,0 \quad (6.49)$$

where $\Phi = 0,5 \left[1 + \alpha (\bar{\lambda} - 0,2) + \bar{\lambda}^2 \right]$

$$\bar{\lambda} = \sqrt{\frac{A f_y}{N_{cr}}} \quad \text{for Class 1, 2 and 3 cross-sections}$$

$$\bar{\lambda} = \sqrt{\frac{A_{eff} f_y}{N_{cr}}} \quad \text{for Class 4 cross-sections}$$

α is an imperfection factor

N_{cr} is the elastic critical force for the relevant buckling mode based on the gross cross sectional properties.

- (2) The imperfection factor α corresponding to the appropriate buckling curve should be obtained from Table 6.1 and Table 6.2.

Table 6.1: Imperfection factors for buckling curves

Buckling curve	a ₀	a	b	c	d
Imperfection factor α	0,13	0,21	0,34	0,49	0,76

- (3) Values of the reduction factor χ for the appropriate non-dimensional slenderness $\bar{\lambda}$ may be obtained from Figure 6.4.

- (4) For slenderness $\bar{\lambda} \leq 0,2$ or for $\frac{N_{Ed}}{N_{cr}} \leq 0,04$ the buckling effects may be ignored and only cross sectional checks apply.

Table 6.2: Selection of buckling curve for a cross-section

Cross section		Limits	Buckling about axis	Buckling curve		
				S 235 S 275 S 355 S 420	S 460	
Rolled sections		$h/b > 1,2$	$t_f \leq 40 \text{ mm}$	y-y z-z	a b	a ₀ a ₀
			$40 \text{ mm} < t_f \leq 100$	y-y z-z	b c	a a
		$h/b \leq 1,2$	$t_f \leq 100 \text{ mm}$	y-y z-z	b c	a a
			$t_f > 100 \text{ mm}$	y-y z-z	d d	c c
Welded I-sections		$t_f \leq 40 \text{ mm}$	y-y z-z	b c	b c	
		$t_f > 40 \text{ mm}$	y-y z-z	c d	c d	
Hollow sections		hot finished	any	a	a ₀	
		cold formed	any	c	c	
Welded box sections		generally (except as below)	any	b	b	
		thick welds: $a > 0,5t_f$ $b/t_f < 30$ $h/t_w < 30$	any	c	c	
U-, T- and solid sections			any	c	c	
L-sections			any	b	b	

Provided by Standard Online AS for Universitetet i Stavanger, TNF 2011-06-24. Reproduction is not allowed.

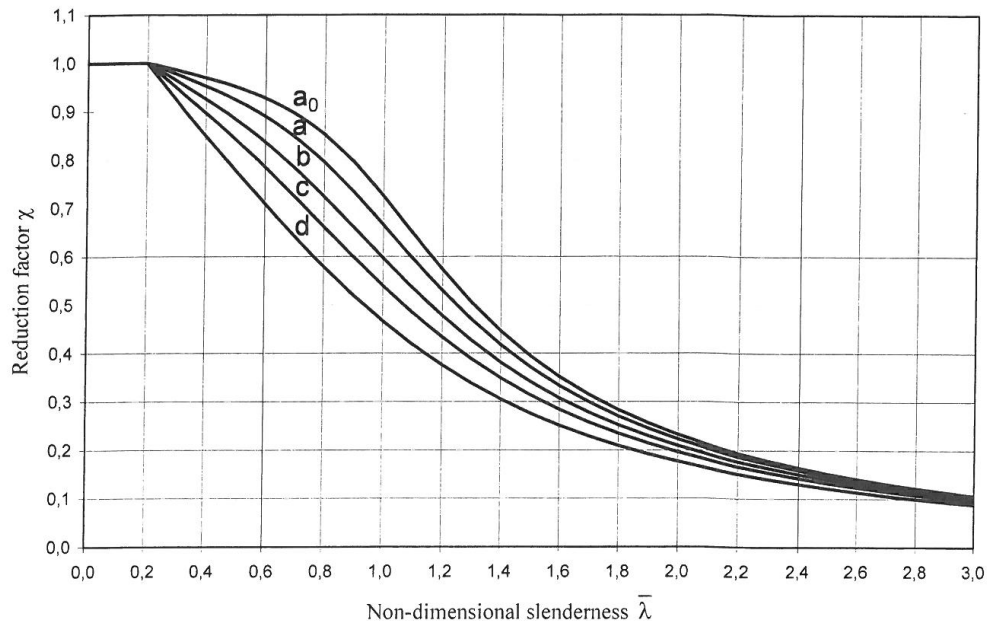


Figure 6.4: Buckling curves

6.3.1.3 Slenderness for flexural buckling

- (1) The non-dimensional slenderness $\bar{\lambda}$ is given by:

$$\bar{\lambda} = \sqrt{\frac{Af_y}{N_{cr}}} = \frac{L_{cr}}{i} \frac{1}{\lambda_1} \quad \text{for Class 1, 2 and 3 cross-sections} \quad (6.50)$$

$$\bar{\lambda} = \sqrt{\frac{A_{eff}f_y}{N_{cr}}} = \frac{L_{cr}}{i} \frac{\sqrt{\frac{A_{eff}}{A}}}{\lambda_1} \quad \text{for Class 4 cross-sections} \quad (6.51)$$

where L_{cr} is the buckling length in the buckling plane considered

i is the radius of gyration about the relevant axis, determined using the properties of the gross cross-section

$$\lambda_1 = \pi \sqrt{\frac{E}{f_y}} = 93,9\varepsilon$$

$$\varepsilon = \sqrt{\frac{235}{f_y}} \quad (f_y \text{ in N/mm}^2)$$

NOTE B For elastic buckling of components of building structures see Annex BB.

- (2) For flexural buckling the appropriate buckling curve should be determined from Table 6.2.